

**PAPER TITLE:**

**Geometric and kinematic characterization of landslides affecting urban areas: the Lungro case study (Calabria, southern Italy)**

**Authors:**

Giovanni Gullà\*, Dario Peduto\*\*, Luigi Borrelli\*, Loredana Antronico\*, Gianfranco Fornaro\*\*\*

\* Research Institute for Geo-Hydrological Protection,

National Research Council of Italy

Via Cavour n. 4/6, 87030, Cosenza, Italy

e-mails: [gulla@irpi.cnr.it](mailto:gulla@irpi.cnr.it); [borrelli@irpi.cnr.it](mailto:borrelli@irpi.cnr.it); [antronico@irpi.cnr.it](mailto:antronico@irpi.cnr.it)

\*\* Department of Civil Engineering, University of Salerno

Via Giovanni Paolo II, 132, 84084 - Fisciano (SA)

Email: [dpeduto@unisa.it](mailto:dpeduto@unisa.it)

\*\*\*

Institute for Electromagnetic Sensing of the Environment (IREA – CNR)

Via Diocleziano 328, 80124 Naples, ITALY

Email: [fornaro.g@irea.cnr.it](mailto:fornaro.g@irea.cnr.it)

**Corresponding author**

Dario Peduto

Department of Civil Engineering, University of Salerno

Via Giovanni Paolo II, 132, 84084 - Fisciano (SA)

Email: [dpeduto@unisa.it](mailto:dpeduto@unisa.it)

Tel. +39 089 964120; Mobile +39 3286935656

**Keywords:** landslides, monitoring, A-DInSAR, kinematics, typifying

**Abstract**

The geometric and kinematic characterization of landslides affecting urban areas is a challenging goal that is routinely pursued via geological/geomorphological method and monitoring of ground displacements achieved by geotechnical and, more recently, advanced differential interferometric synthetic aperture radar (A-DInSAR) data. Although the integration of all the above mentioned methods should be planned *a priori* to be more effective, datasets resulting from the independent use of these different methods are commonly available, thus making crucial the need for their standardized *a posteriori* integration. In this regard, the present paper aims to provide a contribution by introducing a procedure that, taking into account the specific limits of geological/geomorphological analyses and deep/surface ground displacement monitoring via geotechnical and A-DInSAR data, allows the *a posteriori* integration of the results by exploiting their complementarity for landslide characterization. The approach was tested in the urban area of Lungro village (Calabria region, southern Italy), which is characterized by complex geological/geomorphological settings, widespread landslides, and peculiar urban fabric. In spite of the different level of information preliminarily available for each landslide as result of the independent use of the three methods, the implementation of the proposed procedure allowed a better understanding and typifying of the geometry and kinematics of 50 landslides. This provided part of the essential background for geotechnical landslide models to be used for slope stability analysis within landslide risk mitigation strategies.

## **1. INTRODUCTION**

The choice of an appropriate procedure for slope stability analysis, hazard and risk evaluation depends on several key factors such as the scale of analysis (e.g., regional, local or site specific) (Fell et al., 2008); the environmental context (e.g., primarily natural or predominantly urbanized) (Bonci et al. 2010; Booth et al. 2015; Cascini et al. 2006; Ciampalini et al. 2012) and the purpose of the analysis (e.g., emergency, scientific, prevention, control) (Abolmasov et al. 2015; Antronico et al. 2015; Barla

et al. 2010; Borrelli et al. 2014; Gullà et al. 2004; Nico et al. 2015; Pilot 1984; Wang 2012; Yin et al 2010). A fundamental step in this type of studies is the characterization of the geometric and kinematic features of mass movements affecting a given area (Antronico et al. 2013; Baldi et al. 2008; Carter and Bentley 1985; Eberhardt 2008; Grana and Tommasi 2014; Gullà 2014; Maiorano et al. 2015; Uzielli et al. 2015; Vaunat and Leroueil 2002). This step may involve various methods that have been described in the scientific literature (Di Maio et al. 2013; Farina et al. 2006; Fukuoka 1980; Komac et al. 2015; Massey et al. 2013; Shimizu et al. 2014; Wasowski and Bovenga 2014; Willenberg et al. 2008; Yin et al. 2010; Yenes et al. 2009) and whose effectiveness is closely related to the above three factors. In particular, used methods are: the geological-geomorphological (*GeoG*) one, which is mostly effective on a regional scale or over large areas; satellite radar images (*Sat*), which have been successfully used in certain contexts (e.g., monitoring of urbanized areas that are affected by slow-moving landslides); the geotechnical (*Geot*) one, which is essential when working at slope scale. In urban areas in particular, geometric and kinematic landslide characterization is addressed mainly with the independent use of one of the above methods (Antolini et al. 2013; Antronico et al. 2013; Bovenga et al. 2013; Laribi et al. 2015; Simeoni and Mongiovì 2007; Xiao and He 2013; Yenes et al. 2009), which are in some cases integrated without initial planning (Du et al. 2013; Kumsar et al. 2015). In the authors' experience, and with particular reference to current practice, the lack of integration is due to several factors including the need to continually coordinate the activities pertaining to each method, the scarcity of resources at all times, and the different time schedules in designing and implementing the activities of the various methods. However, it is worth stressing that the integration of the three abovementioned methods may increase the effectiveness of the overall results (Antronico et al. 2013; Barla et al. 2010; Bonci et al. 2010; Calò et al. 2012; Tofani et al. 2013a; Uzielli et al. 2015).

In this paper an *a posteriori* integration (*aPosIn*) of the results obtained from *GeoG*, *Sat* and *Geot* methods is applied to the Lungro urban area (Calabria region, southern Italy) that has complex urban fabric and geological/geomorphological settings where landslides are widespread (Fig. 1). As a result,

through the exploitation of the elements of complementarity of the three independent methods it was possible typifying all landslides in the area from both the geometric and kinematic point of view.

## **2. METHODS**

This section provides a quick overview of *GeoG*, *Sat* and *Geot* methods focusing on their limitations and potential as highlighted in the scientific literature referring to their independent use for landslide characterization. Next, the proposed *aPosIn* procedure is outlined.

### **2.1. Geological-geomorphological investigation**

To assess mass movements in an urban area and to define their stability conditions, landslide inventory maps and geological maps can be produced via aerial photograph interpretation and field surveys (*GeoG* method).

With regard to mass movements, it is widely known that the reliability of stereoscopic interpretation primarily depends on the experience of the photo interpreter and on the availability, type and quality of the aerial photographs (Rib and Liang 1978). However, identification and mapping of landslide bodies are particularly complex in urban areas (Guzzetti et al. 2012, and citations therein). Stereoscopic analysis of aerial photos taken at different times allows for the reconstruction of landslide movements in a study area (Walstra et al. 2007; Zanutta et al. 2006). The resulting multi-temporal inventory maps, however, may be limited by, among other factors, the type of movement, changes in the vegetation cover, and the evolution of the urban area (Guzzetti et al. 2012).

Generally, field surveys are useful for mapping landslide events immediately after activation/reactivation and for improving or validating the inventory maps obtained from the interpretation of aerial photographs (Guzzetti et al. 2012, and citations therein).

Moreover, in the case of slow-moving landslides affecting urban areas, field surveys aimed at recording cracks and deformations of buildings and infrastructures can be extremely useful for

determining the instability conditions. In particular, photo comparison of damages to buildings taken at different times can allow for the landslide boundary identification and the landslide activity definition, otherwise not easily mapped through aerial photographs (Antronico et al. 2015).

With regard to geology, a geological map of the study area is paramount for the study of slope instability issues (Borrelli et al. 2014). Also in such case, a detailed geological survey, supported by a preliminary photointerpretation analysis, constitutes the first step in the definition of the geological and structural features and of the geological model of the study area.

## **2.2.Satellite monitoring**

Synthetic Aperture Radars (SAR) are systems able to regularly acquire data over repeated passes. Advanced Differential Interferometric SAR (A-DInSAR) is a technique that processes coherent stacks of SAR images to derive information about the displacements of the ground surface. This is a satellite-based method (*Sat*), able to achieve centimetric to millimetric accuracy and to assess slope stability conditions in urban areas (Cascini et al. 2013a; Cigna et al. 2013; Ferlisi et al. 2014). Available A-DInSAR techniques for the analysis of phase signals in interferometric stacks can be grouped mainly in two classes: persistent scatterers interferometry (PSI) (Costantini et al. 2008; Crosetto et al. 2008; Ferretti et al. 2001) and the small baseline (SBAS) technique (Berardino et al. 2002; Fornaro et al. 2009a). The two methods essentially approach the problem at different scales and are tailored to complementary scattering mechanisms. PSI analyses are performed at full resolution on stable scatterers to filter out the atmospheric disturbances and to retrieve accurate topographic and deformation measurements. Monitored scatterers correspond to man-made structures and infrastructure (e.g., buildings, roads, bridges) or bare rocks that are larger than the system resolution. In the case of SBAS techniques, the scattering is assumed to be distributed within a resolution cell (for instance rural areas) and a spatial multilooking is applied to enhance the phase stability. As a consequence of this technique, the spatial resolution of the product is degraded with respect to that of the PSI approach, but an increase in the density of monitored areas is achieved. A

side product of this small-scale analysis is an estimate of the atmospheric phase delay (APD), which allows for subsequent analysis at full resolution (Fornaro et al. 2009b) to achieve a product at a larger scale as PSI. Conversely, an extension of the PSInSAR technique (Ferretti et al. 2001) that makes use of multilooking during the data processing to extract equivalent PS scatterers also in the presence of distributed scatterers, known as SQUEESAR (Fumagalli et al. 2011), has been recently proposed. The idea behind (see Fornaro et al., 2015) is the decomposition of the covariance matrix associated with the scattering measured at different acquisitions of a multipass/multibaseline stack, into dominant components.

The radar analysis performed in this study was based on a two-step approach. Specifically, a low-resolution analysis (with a pixel spacing of nearly 80 x 80 m) was performed using the original small baseline subset (SBAS) algorithm (Berardino et al. 2002), and then a full-resolution analysis (with a pixel spacing of 20 x 5 m) was performed in accordance with the tomographic analysis technique proposed by Fornaro et al. (2009b). This latter technique consists of a full-resolution analysis capable of also retrieving deformation measurements from targets interfering within the image pixels. This technique was applied in this study to identify the dominant scatterer, as is typical in PSI. According to several studies present in the literature for typical C-band stacks acquired over intervals of more than 4-5 years typical accuracies achieved with A-DInSAR approaches are on the order  $\pm 1$  mm/year for the average velocity and sub centimetric for single displacement measurements. Each coherent pixel is associated with a coherence value (ranging from 0 to 1), which indicates the degree to which the measurement fits the model assumed for the displacement.

A review of the literature yielded (e.g., Wasowski and Bovenga 2014) several papers that address the application of A-DInSAR data (processed using either PSI or SBAS techniques) to the study of slow-moving landslides. These works stress the potential of the techniques to provide information regarding elements (structures and infrastructure) exposed to landslide risk with accuracy comparable to and at lesser cost than conventional monitoring techniques while providing displacement time series spanning more than 20 years since 1992. Three primary current limitations are the following:

(i) sensor revisit times (although these are reduced in the case of very high-resolution X-band SAR sensors such as those of the CosmoSkyMed, see for instance Cascini et al. (2013b), and TerraSAR-X missions as well as for the Sentinel-1 program with the first recently launched satellites) allow for application of the technique to landslides whose velocities – based on the classification of Cruden and Varnes (1996) – range from extremely slow to very slow (Cascini et al. 2009, 2010; Colesanti and Wasowski 2006); for example, using ERS/ENVISAT data (used in the present study), it is possible to track displacements with velocities exceeding 14.5 cm/year with respect to the context (Colesanti and Wasowski 2006); (ii) there is very poor coverage in vegetated areas from sensors operating in the C band (Wei and Sandwell 2010); improved coverage can be obtained from systems operating in the L band, as was recently demonstrated, for example, by Bianchini et al. (2013); (iii) one-dimensional LOS measurements require projection operations to take into account slope and aspect angles, the acquisition geometry of the sensors, and kinematic features of the observed phenomenon (Cascini et al. 2009, 2010, 2013a; Colesanti and Wasowski 2006).

Many authors (Cascini et al. 2009, 2010; Catani et al. 2005; Cigna et al. 2013; Fornaro et al. 2013; Herrera et al. 2013; Lu et al. 2014; Meisina et al. 2008; Notti et al. 2010; Peduto et al. 2015; Tofani et al. 2013b; Wasowski and Bovenga 2014) already investigated the potential of A-DInSAR data for the analysis of different types of slow-moving landslides (Varnes 1978).

Currently, abundant A-DInSAR data are available due to international (Del Ventisette et al. 2013; TERRAFIRMA 2015), national (MATTM 2010) and regional projects (Meisina et al. 2008; Risknat Project 2012; Terranova et al. 2009).

### **2.3. Geotechnical monitoring**

Geotechnical monitoring (*Geot*) of mass movements can be aimed at various objectives, including knowledge, control, and warning (François et al. 2007; Gullà 2014; Massey et al. 2013; Sassa et al. 2009). This approach is well established in urban areas and is performed with the use of increasingly advanced equipment (Bhandari et al. 2013; Kim 2008; Sassa et al. 2009.). The integrated use of

monitoring networks for the measurement of both surficial and deep displacements can provide an adequate characterization of geometric and kinematic features of unstable slopes (Calcaterra et al. 2012; Gullà et al. 2006; Petley et al. 2005; Tommasi et al. 2006). However, in urban areas geotechnical monitoring of ground displacements poses several difficulties, often substantial, that may affect, limit and sometimes prevent its use. Historic centres or other locations, where the configurations of buildings and roads hamper access, bring along additional constraints. Widely shared guidelines for overcoming limitations concerning available instrumentation, measurement procedures and processing techniques still tend to be scarce.

With reference to surface displacement monitoring via GPS systems in urban areas frequent constraints include the following: *(i)* large or contiguous buildings, narrow roads and roads with significant gradients; *(ii)* fixed benchmarks inadvertently positioned in unstable areas; *(iii)* vegetation and/or certain radio frequencies that may disturb the GPS signal reception; *(iv)* difficulty to obtain permission to access specific sites (Bonci et al. 2010; Gili et al. 2000; Shimizu et al. 2014; Wang et al. 2014).

There may be additional limitations when monitoring deep displacements by inclinometers (e.g. presence of underground utility lines, proper positioning of the inclinometer verticals for both sliding surface detection and to kinematic feature retrieval) (Stark and Choi 2008; Wang et al. 2014).

#### **2.4.A *posteriori* integration (*aPosIn*) procedure**

The methods described in the previous sections independently provide data and useful information in urban areas. Recently, to assess surficial displacements induced by slope movements and to delineate the geometry and depth of the sliding surface, procedures combining landslide inventory maps (resulting from geomorphological investigations), surficial displacement data (e.g. acquired from spaceborne radar sensors and GPS measurements) and measurements of ground displacements (e.g. inclinometer readings) have been proposed with reference to single landslides (Antolini et al. 2013; Farina et al. 2006; Tofani et al. 2013a).



However, a general framework for a systematic integration of the results of *GeoG*, *Sat* and *Geot* methods for landslide characterization in urban area is not yet available. The present paper makes an attempt in this direction by proposing the procedure synthesized in Figure 2 pursuing the *a posteriori* integration (*aPosIn*) of either two or all the above mentioned methods. This integration procedure consists of three phases.

First (Phase I), the results pertaining to the study area are mapped and analysed. In particular, landslides identified using *GeoG* method are classified in categories, referring to their lithology, maximum thickness, kinematic features, and state of activity; each zone of the urban area covered by *Sat* data is assigned an average yearly velocity value; each site of the urban area for which *Geot* monitoring data are available is assigned a yearly velocity value and maximum thickness.

In the second phase (Phase II), the results from coupling two methods are mutually validated and integrated; the possible combinations are *GeoG U Sat*, *GeoG U Geot*, and *Sat U Geot*. In particular, movement information derived from either *GeoG* or *Sat* methods are compared and integrated; further checks are carried out concerning the boundaries of the mapped phenomena via *GeoG* method and the position of *Sat* data exhibiting conditions of movement. Then, information on thickness of landslides is derived from the merge of *GeoG* and *Geot* method. Finally, measured displacement velocities retrieved from either *Sat* or *Geot* method are assigned to classes ( $VeC_{ith}$ ) corresponding to ranges of average yearly velocity moduli based on expert knowledge of the study area.

In Phase III the results from all three methods are integrated: *GeoG U Sat U Geot* (Fig. 2). In particular, landslides for which the outcomes of the *GeoG*, *Sat* and *Geot* methods are available are first typified in terms of: involved lithology and type, geometric (e.g. length,  $L$ ; width,  $W$ ; depth of sliding surface) and kinematic (e.g. average yearly velocity) characteristics. Then, they are assigned to categories which can differ from the ones defined only according to the *GeoG* method. Finally, all the remaining landslides in the study area are reclassified by taking into account similarities of their morphometric parameters (e.g.  $L$  and  $L/W$  ratios) with the other phenomena already typified.

### **3. RESULTS**

The *aPosIn* procedure was applied to the Lungro urban area that can be distinguished in four different zones according to geomorphological features and urban fabric characteristics (Fig. 1): Historic centre (HC); Carmine (CA); Lafcantino (LA); San Leonardo (SL).

#### **3.1. Phase I**

The Phase I of the procedure consisted of the analysis and mapping of the results obtained from the independent application of each method (Fig. 2).

##### *3.1.1 GeoG method*

From a geological point of view (Fig. 1), the north-western portion of the area is characterized by the presence of the Lungro-Verbicaro Unit, dating back to the Middle Trias, made up of metapelites and metacarbonates (Iannace et al. 2005). The Lungro-Verbicaro Unit, next to the dwelled area of Lungro, moves towards the Ophiolitic Unit of Diamante-Terranova (Lower Jurassic-Cretaceous), with a clear extensional tectonic contact. In particular, the cover of the Diamante-Terranova Unit, made up of phyllites and slates, crops out in the study area. Overall these lithotypes form a “melange structure” made up of blocks and fragments of different nature (e.g., phyllites, slates and metacarbonates) in a prevalently clayey matrix, derived from the degradation of phyllites (Antronico et al. 2015, 2013).

The metasediments of the Diamante-Terranova Unit are overlain by an Upper Tortonian–Messinian sequence composed of coarse sandstone and shale interbedded with gypsiferous sandstone and gypsum. The Early Miocene succession then ends with deposits dating to the Middle Pliocene–Pleistocene, represented by sandy and conglomeratic beds. Colluvium and landslide debris, with a maximum thickness of approximately 10 meters, mantle the phyllite bedrock on the slopes (Fig. 1) (Antronico et al. 2013).

A landslide inventory map of the study area was prepared using aerial photographs acquired in 1955 (scale 1:33,000), 1980 (scale 1:25,000), 1991 (scale 1:33,000), 2001 (scale 1:15,000), and field surveys (Fig. 3a). The area is affected by a large number of landslides of various types that were classified with reference to Varnes (1978).

The carbonate hillslopes are characterized by sub-vertical scarps and are affected by small toppling and rockfalls. In this area (La Petrosa), an arcuate and degraded scarp marks the upslope margin of an ancient rock block slide (Antronico et al. 2013). These features may explain the presence of carbonate blocks larger than 1 m<sup>3</sup> forming a debris deposit more than 10 m thick, outcropping in the south-western part of the Historic centre (namely HC in Figs. 1 and 3a).

The phyllite hillslopes are extensively affected by several mass movements (Fig. 3): slide, complex slide/flow (Varnes 1978) and landslide zone (Greco et al. 2007). This latter represents an area where clustering of mass movements (slides, complex slide/flows) is so tight that it is impossible to distinguish the different bodies, but sometimes landslide phenomena can be mapped inside the area. Based on the depth (estimated on a geomorphological basis), the involved lithologies and the type of the landslides, the following four landslide categories were established: (i) category A landslides, whose type can be ascribed to complex landslides, are shallower than 10 m and affect detrital-colluvial covers; (ii) category B landslides, extending to depths between 10 m and 20 m, affect deeply weathered and chaotic phyllites and belong to the complex landslides type; (iii) category C landslides, extending to depths between 20 m and 30 m, affect deeply weathered and chaotic phyllites and belong to the landslide zone; (iv) category D landslides, extending to depths between 20 m and 30 m, affect weathered and chaotic phyllites and belong to the slide type.

In the study area, the majority of landslides show evidence of recurrent activity. The analysis of historic data spanning from 1812 and 2005 indicates that the HC of Lungro and nearby newly developed areas (CA, LA, SL) were intermittently affected by landslide phenomena, generally slow ones, that severely impacted local social development and business activities (Gullà et al. 2006).

Evidence of landslide activity in the study area includes cracks in houses and distortion of roads (Antronico et al. 2015).

### *3.1.2 Sat method*

The image dataset used in the present study consists of 64 ENVISAT images acquired on both ascending (no. 35, track 86, frame 783, 27 August 2003 to 27 January 2010) and descending (no. 29, track 222, frame 2817, 4 May 2003 to 21 February 2010) orbits.

In Phase I a preliminary analysis of the A-DInSAR data over the Lungro area exploited low-resolution data (Fornaro et al. 2009a) without taking into account information from available thematic maps or ground monitoring data. Indeed, as described by Cascini et al. (2010), the analysis of low-resolution A-DInSAR data can be valuable for gathering a general understanding of the features and kinematics across the study area (Fig. 4a). Lungro area contains 81 low-resolution A-DInSAR coherent pixels (with average dimensions of 80 x 80 m), based on ENVISAT data. In particular, 8 pixels from a descending orbit (denoted by black contoured circles) and 73 from an ascending orbit (denoted by circles) correspond to the crests of the local relief, which are densely urbanised. The majority of coherent pixels on ascending orbits can be attributed to slopes that primarily face east. Moreover, coherent pixels exceeding the movement threshold based on the LOS velocity (i.e., 1.5 mm/year, Cascini et al., 2009) are widespread in built-up areas across the municipal territory, with higher concentrations in HC and LA and additional sparse data bordering CA and SL.

Since the present study was performed in an urban area, an additional step involved the use of full-resolution A-DInSAR data. These data better fit analyses on a detailed scale (i.e., 1:5000; 1:1000) for defining the boundaries and the state of activity of slow-moving landslides and the monitoring of affected facilities (Cascini et al. 2013a).

In agreement with the outcomes of low-resolution A-DInSAR data analysis, full-resolution A-DInSAR data indicate that, although most of the A-DInSAR data provides evidence of movements across all of the area, certain portions exhibiting higher velocities can be identified. In Fig. 4b, the

superimposition of full-resolution A-DInSAR data (128 on descending and 908 on ascending orbits) allows for the portions of Lungro with the highest concentration of “moving” pixels to be identified. Apart from HC, which is fully covered by moving A-DInSAR pixels, in LA, CA and SL, moving pixels concentrate along a road located at the crest of the slope where several buildings are located. Table 1 presents details of recorded A-DInSAR velocities indicating that most of the moving pixels are within HC and LA, with average LOS velocity moduli reaching 0.45 cm/year and 0.41 cm/year, respectively.

### *3.1.3 Geot method*

The results of *Geot* method were obtained from two monitoring networks: GPS for absolute surface displacements and vertical inclinometers for measurements also of deep displacements (Fig. 5).

The GPS monitoring network included 9 benchmarks located as follows: two in HC, two in LA, four in CA, and one in SL. The measurements were performed at all nine measuring points from June 2006 till May 2007. Then, due to damage, from October 2008 to October 2011, only seven benchmarks were functional.

The yearly average and maximum velocities of each GPS were calculated and assigned to classes as shown in Figs. 5a-b. The average and maximum velocities of the benchmarks in CA and SL primarily are 3-30 cm/year and more than 100 cm/year, respectively. In HC and LA, the average velocities range from 0.5 to 3 cm/year up to 100 cm/year, and the maximum velocities values range from 3 to 30 cm/year up to more than 100 cm/year.

Deep ground displacement measurements were performed using a network of 12 vertical inclinometers, whose positions were selected based on the characteristics of the urban fabric (Figs. 5c-d). The inclinometer data were collected from 2006 to 2011 between depths of 25 m and 80 m. Figs. 5c-d show the yearly average and maximum velocities at a depth of 1 m and their assignments to the same classes as those of the GPS measurements. In CA and SL, both the yearly average and

maximum velocities generally exceed 3 cm/year, whereas the velocities in HC and LA rarely exceed 3 cm/year.

The inclinometric data show displacement trends with depth and the thicknesses of the unstable rock masses (Fig. 6).

Displacements in HC are generally constant with depth, sharp and well defined. The deepest sliding surfaces are located at depths of approximately 20-30 m, except at inclinometer S03 where the shear plane is much shallower (6 m). Two inclinometers (S19 and S20) show multiple sliding surfaces (Fig. 6). In LA, inclinometer S04 shows extremely small displacements and a barely distinguishable sliding surface at approximately 25-30 m. In CA, inclinometer S10 intercepts a well-defined sliding surface at a depth of 10 m. In SL, clear sliding surfaces are distinguished at depths of approximately 12-16 m.

The minimum, average and maximum velocities at the 1-m depth are summarized in Table 2. Except for inclinometer F03, for which only one velocity is available, the minimum velocities range from 0.03 cm/year (S20 in HC) to approximately 6 cm/year (S09 in SL), the average velocities range from 0.18 cm/year (S22 in HC) to 18 cm/year (F13 in SL), and the maximum velocities range from 0.35 cm/year (S22 in HC) to approximately 51 cm/year (F13 in SL). These results indicate extremely slow to very slow displacements (Varnes 1978) during the period of 2006-2011.

### **3.2. Phase II**

Following the criteria described in section 2.4, in the Phase II, average yearly velocity classes were assumed based on previous studies performed in the Lungro urban area (Antronico et al. 2015, 2013). Table 3 shows the six selected classes:  $VeC_1$  to  $VeC_3$  coincide with the moduli of A-DInSAR velocity classes;  $VeC_4$  to  $VeC_6$  were defined according to Antronico et al. (2015).

Then, the results of the *GeoG* method were merged with those of the *Sat* method (Fig. 7a). In HC, three velocity classes ( $VeC_{ith}$ ) for low-resolution A-DInSAR coherent pixels can be distinguished (Fig. 7a):  $VeC_4$  is present within two active landslides (12) and (18), both belonging to category D;

$VeC_3$  is recorded in landslide (18) and on the landslide debris detected in the western portion of HC (Fig. 3a). North and south of HC, two zones with predominantly  $VeC_2$  were identified: the northern zone borders the flank and crown of landslide (18), and the southern zone is near the crown of landslide (9).

In LA, which extends north-west to south-east primarily along a crest, the zones containing low-resolution A-DInSAR data are located mainly near a few landslide crowns mapped in LA, CA and SL. In particular, in the north-western part of LA,  $VeC_3$  is recorded near landslide zone (26). To the east, the low-resolution A-DInSAR coherent pixels belong to class  $VeC_2$ . To the south-east,  $VeC_3$  is present near the crown of landslide (25) that has the active portion (45). Finally,  $VeC_4$  provides evidence of movement where no landslides - except for the crown of a landslide (16) - were mapped. In CA, there are only few low-resolution A-DInSAR coherent pixels; whereas no pixels are available in SL.

Additional detail was provided by an analysis of the full-resolution A-DInSAR data (Fig. 7b). In particular, in the northern portion of HC – where no landslides were mapped – the full-resolution A-DInSAR data yielded velocities of class  $VeC_1$ , thus confirming that this area is stable. In contrast, over landslides (12) and (18),  $VeC_4$  is recorded.  $VeC_3$  concentrates in the western portion of landslide (18) in Fig. 7b. In the western portion of HC there are widespread full-resolution A-DInSAR coherent pixels belonging to class  $VeC_3$  and  $VeC_2$  pixels are randomly distributed (Fig. 7b).

In the north-western portion of LA, near the boundaries of landslide zone (26) mainly  $VeC_3$  and  $VeC_4$  are recorded. South-east of LA,  $VeC_4$  prevails along the crest and near landslides (25), (45), (43), (42) and (16), Fig. 7b.

In CA there is a small number of full-resolution A-DInSAR coherent pixels. In particular,  $VeC_4$  concentrates on landslide (31) and the other classes sparsely cover the upper portion of landslide (26). A small number of class  $VeC_4$  full-resolution A-DInSAR coherent pixels are located near the upper boundary of landslide (0) in the SL.

The integration of the results obtained using the *GeoG* and *Geot* methods is shown in Fig. 8.

In HC, 5 inclinometers in landslide (18) exhibit displacements with average yearly velocities belonging to *VeC\_4*. Similar information is provided by GPS12, which is located in landslide (12). Moreover, inclinometers S22 and S21 mark a transition between *VeC\_4* and *VeC\_2* (Fig. 8a); inclinometer S03 and GPS11 indicate *VeC\_4* in landslide (47).

In LA, inclinometer S04 indicates *VeC\_2* in landslide (23) (Fig. 8a). GPS9, near the boundaries of landslide (45), yields *VeC\_5*, and GPS2, located in landslide (42) records *VeC\_6*.

In CA, inclinometer S10, located in landslide (37), records *VeC\_5* (Fig. 8a); whereas four GPS yield velocities of class *VeC\_6*: GPS7 in landslide (26), GPS6 in landslide (32), and GPS4 and GPS5 in landslide (37).

In SL, inclinometers F03 and F13 and GPS3, located at the head of landslide (0), yield velocities of class *VeC\_6*, whereas inclinometer S09, located in the central portion of the landslide, shows a slightly slower displacement (*VeC\_5*).

Inclinometers (see Fig. 6) also provide information about the thicknesses of the unstable masses, as shown in Fig. 8b.

The integration of the results from the *Sat* and *Geot* methods is shown in Fig. 9.

In HC, the velocities obtained from A-DInSAR, inclinometers and GPS monitoring clearly match in that they belong to *VeC\_4*.

In the other areas, the inclinometers and GPS measurements complement the A-DInSAR data where the latter are not available due to excessively high velocities (causing a loss of coherence) and an absence of targets (e.g., buildings and roads).

### **3.3. Phase III**

With regards to Phase III the integration of the results from the three methods is preliminarily shown in Fig. 10.

In HC, the activity of landslides (12) and (18), defined from *GeoG* result, was confirmed by both *Sat* and *Geot* results. Between landslides (18) and (12), progressively west to east and downslope,



different conditions of movement are detected, with a well-defined transition zone from *VeC\_3* to *VeC\_4*. In this area, the landslides are mainly characterized by sliding surfaces at depths ranging from 6 m up to about 30 m.

In LA, the integration of all available results allows for the identification of possible reactivation and retrogression of dormant landslides (e.g., landslides 25 and 16).

In CA and SL, the integration of the results helped to overcome the constraints related to the peculiar characteristics of the urban fabric (i.e., a few scattered buildings and extremely difficult access to the areas near zones of interest) and certain method-specific limitations (loss of coherence in the A-DInSAR data due to excessively high velocities; see section 2.2). As a result, in CA the landslides are primarily characterized by velocities of classes *VeC\_5* and *VeC\_6* and sliding surfaces at depths of approximately 10 m; in SL specific information concerns landslide (0) which is active with velocities of classes *VeC\_5* and *VeC\_6* – the latter were recorded near the crown – and sliding surface at depths of 12-16 m.

Then proceeding with the integration process, the category assigned to each landslides based on *GeoG* method was checked and better defined (i.e. from category A to category T\_Ai, from category B to category T\_Bi, from category C to category T\_Ci, from category D to category T\_Di).

As a result landslides (42) and (47) (Fig. 10), previously included in category A, were assigned to category T\_A1 (Fig. 11), which is characterized by a length (*L*) to width (*W*) ratio of approximately 2, a maximum depth of approximately 6 m, and velocities ranging from 2 to 4 cm/year (average) to more than 200 cm/year (maximum), which are indicative of possible pre-failure or failure phases. Landslide (45), also belonging to category A (Fig. 10), was assigned to category T\_A2 (Fig. 11) and exhibits a *L/W* ratio of approximately 4.5, a maximum depth of approximately 10 m and velocities ranging from 5 to 7 cm/year (average) to more than 20 cm/year (maximum). Landslides (42) and (47) (category T\_A1) and landslide (45) (category T\_A2), which are of the complex type, both affect detrital-colluvial covers.

Landslides (31) and (32) (Fig. 10) (category B) were assigned to category T\_B1 (Fig. 11) based on the following geometric and kinematic features:  $L/W$  ratio of approximately 2, maximum depth of approximately 10-20 m, and velocities ranging from 0.5 to 5 cm/year (average) to more than 80 cm/year (maximum). Landslides (0) and (37) (also belonging to category B) were assigned to category T\_B2 based on their  $L/W$  ratios of approximately 2.5, maximum depths of approximately 10-16 m (Fig. 11), and velocities ranging from 4 to 20 cm/year (average) to more than 100 cm/year (maximum). Landslides (31), (32), (0), and (37) are all of the complex type and affect deeply weathered and chaotic phyllites.

Landslide (26) (Figs. 10-11), included in category C, was assigned to category T\_C and is approximately 800 m wide, 1500 m long, and 20 to 30 m deep. The kinematic features are characterized by velocities in the range of 0.5-5 cm/year (average) to more than 40 cm/year (maximum).

Finally, landslides (12) and (18) (Figs. 10-11) included in category D were assigned to category T\_D and are, respectively, 100 m and 250 m wide, 350 m and 500 m long and 20-30 m deep. In T\_D category, other failure surfaces can be identified at depths of approximately 10-15 m. They exhibit velocities ranging from 0.2 to 0.5 cm/year (average) to 2-5 cm/year (maximum).

The comparison between Figures 3 and 10 highlights the potential of the *aPosIn* procedure for better defining geometry and kinematics of the analyzed phenomena. In particular, out of 50 landslides characterized via *GeoG* method, the *aPosIn* procedure allowed 10 landslides (labelled in red in Fig. 11) to be directly typified from both the geometric (i.e. boundaries and thickness) and kinematic (i.e. type of movement, velocity class associated with fixed ranges) point of view. These landslides are distributed as follows (Fig. 11): 3 (out of 10) in HC; 2 (out of 11) in LA; 4 (out of 26) in CA; 1 (out of 2) in SL. As for landslide (18) in HC (Fig. 6), useful insights concerning different velocities and the presence of multiple sliding surfaces were achieved.

Starting from the six landslide categories derived from the landslides directly typified, all the other landslides (labelled in black in Fig. 11) were typified based on similar morphometric parameters ( $L$

and  $L/W$  ratios) (Fig. 11). Thus operating, it was possible to distinguish: 14 landslides T\_A1 (i.e. 3 in HC, 3 in LA, 7 in CA and 1 in SL); 18 landslides T\_A2 (i.e. 3 in HC, 5 in LA and 10 in CA); 10 landslides T\_B1 (3 in LA e 7 in CA); 5 landslides T\_B2 (2 in HC, 1 in LA, 1 in CA and 1 in SL); 1 landslide zone T\_C in CA; 2 landslides T\_D in HC.

#### 4. DISCUSSION AND CONCLUSION

With reference to Lungro urban area the analyses carried out confirmed the constraints relevant to *GeoG*, *Sat* and *Geot* methods. For instance, *GeoG* method did not allow proper mapping of landslide boundaries (e.g. landslides 12 and 18) in HC due to their extremely slow kinematics and the presence of dense urbanization. *Sat* method furnished very poor information where coherent pixel coverage was scarce (e.g. in LA and CA) or the recorded velocity were too high, resulting in a loss of coherence (e.g. in SL). Also the *Geot* method proved not suitable in specific portions of Lungro urban area (e.g. in SL) where very high recorded landslide displacements made some inclinometers operative just for a limited period of time (e.g. F03\_SL for about one month and S09\_SL for about 2.5 months).

Notwithstanding the above limits, *GeoG* method allowed the definition of lithology, boundaries, thickness, type and state of activity for all the 50 landslides present in the urban area; *Sat* method allowed zoning portions of the urban area with different average yearly velocity; *Geot* method provided information on displacement rates and thickness of the unstable volumes with reference to the monitored sites.

The implementation of the *aPosIn* procedure contributed to overcome the constraints specific to the independent use of the three methods by taking advantage of their peculiar elements of complementarity (e.g. validation of landslide boundaries in HC, assignment of velocity classes and thickness to landslides). In particular, a significant knowledge improvement for the geometric and kinematic characterization was achieved via the direct typifying of 10 landslides and, then, the subsequent typifying of all the 50 landslides in Lungro urban area according to morphometric

similarities. The result obtained for the Lungro case study shows that the *aPosIn* procedure can be a powerful tool for knowledge synthesis in urban areas that are extensively affected by landslide phenomena and where planning the execution and management of risk mitigation measures turns out to be a major priority.

It is worth stressing that the obtained results could be systematically updated by taking into account further *GeoG* surveys, new *Sat* data - acquired via ultimate sensors providing a remarkably increased ground information in terms of both spatial and temporal coverage - and *Geot* data achieved as result of in-depth analyses of single phenomena.

Moreover, jointly with the characterization of both the pore pressure regime and representative shear strengths, the result concerning the categories of landslides typified via the *aPosIn* procedure could be helpful for the development of geotechnical models of single landslides. Such geotechnical models represent key input data for quantitative landslide risk analyses and for the design of appropriate risk mitigation measures.

The obtained result could represent a useful reference for the geometric and kinematic characterization of landslides in urban areas with similar geological/geomorphological settings to Lungro area. Furthermore, the use of the *aPosIn* procedure may constitute a best practice for urban areas with highly complex geology, geomorphology and urban fabric for which results coming from the independent implementation of *GeoG*, *Sat* and *Geot* methods are available.

## **Acknowledgements**

This work was carried out under the *Commessa TA.P05.012 “Tipizzazione di eventi naturali e antropici ad elevato impatto sociale ed economico”* of the CNR Department “*Scienze del sistema Terra e Tecnologie per l’Ambiente*”. Facilities have been implemented within the framework of the activities of the Civil Protection System of the Regione Calabria. The SAR image dataset used in the paper was provided by European Space Agency under the CAT-1 Project “*Calibration of the Synthetic Aperture Radar (SAR) measures with Integrated Monitoring Networks (IMoN)*”, and *This is a post-peer-review, pre-copyedit version of an article published in LANDSLIDES. The final authenticated version is available online at: <http://dx.doi.org/10.1007/s10346-015-0676-0>*

*Geometric and kinematic characterization of landslides affecting urban areas: the Lungro case study (Calabria, Southern Italy). Gullà G., Peduto D., Borrelli L., Antronico L., Fornaro G. (2017) extended uses in homogeneous geological contexts” (C1P.5618). The authors wish to thank Luigi Aceto, Claudio Reali, Salvatore Guardia, Enzo Valente for their technical support to the geotechnical monitoring.*

## **References**

- Abolmasov B, Milenković S, Marjanović M, Durić U, Jelisavac B (2015) A geotechnical model of the Umka landslide with reference to landslides in weathered Neogene marls in Serbia. *Landslides* 12:689-702
- Antolini F, Tofani V, Del Ventisette C, Luzi G, Casagli N, Moretti S (2013) SAR Interferometry for Landslides Risk Assessment at Local Scale: The Case Study of Castagnola (Northern Apennines, Italy). In: Margottini C. et al. (eds) *Landslide science and practice, volume 2: early warning, instrumentation and monitoring*. Springer, Berlin, pp 407-414
- Antronico L, Borrelli L, Coscarelli R, Gullà G (2015) Time evolution of landslide damages to buildings: the case study of Lungro (Calabria, southern Italy). *Bull Eng Geol Environ* 74:47-59
- Antronico L, Borrelli L, Peduto D, Fornaro G, Gullà G, Paglia L, Zeni G (2013) Conventional and innovative techniques for the monitoring of displacements in landslide affected area. In: Margottini C. et al. (eds) *Landslide science and practice, volume 2: early warning, instrumentation and monitoring*. Springer, Berlin, pp 125-131
- Baldi P, Cenni N, Fabris M, Zanutta A (2008) Kinematics of a landslide derived from archival photogrammetry and GPS data. *Geomorphology* 102:435-444
- Barla G, Antolini F, Barla M, Mensi E, Piovano G (2010) Monitoring of the Beauregard landslide (Aosta Valley, Italy) using advanced and conventional techniques. *Eng Geol* 116:218-235
- Bhandari RK, Cascini L, Peduto D (2013). *Landslide Instrumentation and Monitoring*. In: *Landslide Science and Practice: Early Warning, Instrumentation and Monitoring*. Proc. of 2nd World Landslide Forum, WLF 2011; Rome; Italy; 3 October 2011 - 9 October 2011, Vol. 2, 2013, Pages 1-2, ISBN 978-3-642-31444-5
- Berardino P, Fornaro G, Lanari R, Sansosti E (2002) A New Algorithm for Surface Deformation Monitoring based on Small Baseline Differential SAR Interferograms. *IEEE Trans Geosci Remote Sens* 40:2375-2383
- Bianchini S, Herrera G, Mateos RM, Notti D, Garcia I, Mora O, Moretti S (2013) Landslide activity maps generation by means of Persistent Scatterer Interferometry. *Remote Sens* 5:6198-6222
- Bonci L, Calcaterra S, Cesi C, Gambino P, Gullà G, Niceforo D, Merli K, Sorriso-Valvo M (2010) Displacements on a slope affected by deep-seated Garvitational Slope Deformation: Greci slope (Lago, Calabria, Italy). *Geogr Fis Din Quat* 33:141-153
- Booth AM, Dehls J, Eiken T, Fischer L, Hermanns RL, Oppikofer T (2015) Integrating diverse geologic and geodetic observations to determine failure mechanisms and deformation rates across a large bedrock landslide complex: the Osmundneset landslide, Sogn og Fjordane, Norway. *Landslides* 12:745-756
- Borrelli L, Antronico L, Gullà G, Sorriso-Valvo GM (2014) Geology, geomorphology and dynamics of the 15 February 2010 Maierato landslide (Calabria, Italy). *Geomorphology* 208:50-73
- Bovenga F, Nitti DO, Fornaro G, Radicioni F, Stoppini A, Brigante R (2013) Using C/X-band SAR interferometry and GNSS measurements for the Assisi landslide analysis. *Int J Rem Sen* 34:4083-4104

- Geometric and kinematic characterization of landslides affecting urban areas: the Lungro case study (Calabria, Southern Italy). Gullà G., Peduto D., Borrelli L., Antronico L., Fornaro G. (2017)*
- Calcaterra S, Cesi C, Di Maio C, Gambino P, Merli K, Vallario M, Vassallo R (2012) Surface displacements of two landslides evaluated by GPS and inclinometer systems: a case study in Southern Appennines, Italy. *Nat Hazard* 61:257-266
- Calò F, Calcaterra D, Iodice A, Parise M, Ramondini M (2012) Assessing the activity of a large landslide in southern Italy by ground-monitoring and SAR interferometric techniques. *Int J Rem Sen* 33:3512-3530
- Carter M., Bentley SP (1985) The geometry of slip surfaces beneath landslides: Predictions from surface measurements. *Can Geotech J* 22:234–238
- Cascini L, Fornaro G, Peduto D (2009) Analysis at medium scale of low-resolution DInSAR data in slow-moving landslide affected areas. *ISPRS J Photogram Remote Sens* 64:598-611
- Cascini L, Fornaro G, Peduto D (2010) Advanced low- and fullresolution DInSAR map generation for slow-moving landslide analysis at different scales. *Eng Geol* 112:29-42
- Cascini L, Gullà G, Sorbino G (2006) Groundwater modelling of a weathered gneissic cover. *Can. Geot. Journal* 43:1153-1166
- Cascini L, Peduto D, Pisciotta G, Arena L, Ferlisi S, Fornaro G (2013a) The combination of DInSAR and facility damage data for the updating of slow-moving landslide inventory maps at medium scale. *Nat Hazards Earth Syst Sci* 13:1527-1549
- Cascini L, Peduto D, Reale D, Arena L, Ferlisi S, Verde S, Fornaro G (2013b) Detection and monitoring of facilities exposed to subsidence phenomena via past and current generation SAR sensors. *J Geophys Eng* 10:1-14
- Catani F, Casagli N, Ermini L, Righini G, Menduni G (2005) Landslide hazard and risk mapping at catchment scale 2005 Arno River basin. *Landslides* 2:329-342
- Ciampalini A, Cigna F, Del Ventisette C, Moretti S, Liguori V, Casagli N (2012) Integrated geomorphological mapping in the north-western sector of Agrigento (Italy). *JoM* 8:136-145
- Cigna F, Bianchini S, Casagli N (2013) How to assess landslide activity and intensity with Persistent Scatterer Interferometry (PSI): the PSI-based matrix approach. *Landslides* 10:267-283
- Colesanti C, Wasowski J (2006) Investigating landslides with spaceborne Synthetic Aperture Radar (SAR) interferometry. *Eng Geol* 88:173-199
- Costantini M, Falco S, Malvarosa F, Minati F (2008) A new method for identification and analysis of persistent scatterers in series of SAR images. *IEEE International Geoscience & Remote Sensing Symposium*, July 6-11, 2008, Boston, Massachusetts, USA, pp 449-452
- Crosetto M, Biescas E, Duro J (2008) Generation of advanced ERS and Envisat interferometric SAR products using the stable point network technique. *Photogram Eng Remote Sens* 4:443-450
- Cruden DM, Varnes DJ (1996) Landslides Types and Processes, in: *Landslides: Investigation and Mitigation*, edited by: Turner, A. K. and Schuster, R. L., Washington DC, Transportation Research Board, National Academy of Sciences, Special Report 247, pp 36-75
- Del Ventisette C, Ciampalini A, Manunta M, Calò F, Paglia L, Ardizzone F, Mondini AC, Reichenbach P, Mateos RM, Bianchini S, Garcia I, Füsü B, Deák ZV, Rádi K, Graniczny M, Kowalski Z, Piatkowska A, Przylucka M, Retzo H, Strozzi T, Colombo D, Mora O, Sánchez F, Herrera G,
- This is a post-peer-review, pre-copyedit version of an article published in **LANDSLIDES**. The final authenticated version is available online at: <http://dx.doi.org/10.1007/s10346-015-0676-0>*

*Geometric and kinematic characterization of landslides affecting urban areas: the Lungro case study (Calabria, Southern Italy). Gullà G., Peduto D., Borrelli L., Antronico L., Fornaro G. (2017)*

Moretti S, Casagli N, Guzzetti F (2013) Exploitation of Large Archives of ERS and ENVISAT C-Band SAR Data to Characterize Ground Deformations. *Remote Sens* 5:3896-3917

Di Maio C, Vassallo R, Vallario M (2013) Plastic and viscous shear displacements of a deep and very slow landslide in stiff clay formation. *Eng Geol* 162:53-66

Du J, Yin K, Lacasse S (2013) Displacement prediction in colluvial landslides, Three Gorges Reservoir, China. *Landslides* 10:203-218

Eberhardt E (2008) Twenty-ninth Canadian Geotechnical Colloquium: The role of advanced numerical methods and geotechnical field measurements in understanding complex deep-seated rock slope failure mechanisms. *Can Geotech J* 45:484-510

Farina P, Colombo D, Fumagalli A, Marks F, Moretti S (2006) Permanent Scatterers for landslide investigations: outcomes from the ESA-SLAM project. *Eng Geol* 88:200-217

Fell R, Corominas J, Bonnard Ch, Cascini L, Leroi E, Savage WZ (2008) Guidelines for landslide susceptibility, hazard and risk zoning for land-use planning, Commentary. *Eng Geol* 102:85-98

Ferlisi S, Peduto D, Gullà G, Nicodemo G, Borrelli L, Fornaro G (2014) The use of DInSAR data for the analysis of building damage induced by slow-moving landslides. In: G. Lollino et al. (eds.), *Engineering Geology for Society and Territory*, Springer International Publishing Switzerland Vol.2, pp 1835-1839. doi: 10.1007/978-3-319-09057-3

Ferretti A, Prati C, Rocca F (2001) Permanent scatterers in SAR interferometry. *IEEE Trans Geosci Remote Sens* 39:8-20

Fornaro G, Nitti DO, Nutricato R, Bovenga F, Peduto D, Cascini L (2013) Technological and Methodological Advances in the Application of Spaceborne DInSAR for Landslide Monitoring. In *Landslide Science and Practice Proceedings of The Second World Landslide Forum*, 3-9 October 2011, Rome. (pp 379-384) Springer Berlin Heidelberg

Fornaro G, Pauciuolo A, Serafino F (2009a) Deformation monitoring over large areas with multipass differential SAR interferometry: a new approach based on the use of spatial differences. *Int J Remote Sens* 30:1455-1478

Fornaro G, Reale D, Serafino F (2009b) Four-dimensional SAR imaging for height estimation and monitoring of single and double scatterers. *IEEE Trans Geosci Remote Sens* 47:224-237

Fornaro G, Verde S, Reale D, Pauciuolo A (2015) CAESAR: An Approach Based on Covariance Matrix Decomposition to Improve Multibaseline/Multitemporal Interferometric SAR Processing. *IEEE Trans. Geosci. Remote Sens.*, 53(4): 2050–2065

François B, Tacher L, Bonnard Ch, Laloui L, Triguero V (2007) Numerical modelling of the hydrogeological and geomechanical behaviour of a large slope movement: the Triesenberg landslide (Lichtenstein). *Can Geotech J*, 44:840-857

Fukuoka M (1980) "Static and Dynamic Earth Pressures on Retaining Walls." Proc. of the 3th Australia-New Zealand Conference of Geomechanics, Wellington, New Zealand

Fumagalli A, Novali F, Prati C, Rocca F, Rucci A (2011) A New Algorithm for Processing Interferometric Data-Stacks: SqueeSAR. *IEEE Trans Geosci Remote Sens* 49:3460-3470



*Geometric and kinematic characterization of landslides affecting urban areas: the Lungro case study (Calabria, Southern Italy). Gullà G., Peduto D., Borrelli L., Antronico L., Fornaro G. (2017)*

Gili JA, Corominas J, Ruis J (2000) Using Global Positioning System techniques in landslide monitoring. *Eng Geol* 55:167-192

Grana V, Tommasi P (2014) A deep-seated slow movement controlled by structural setting in marly formations of Central Italy. *Landslides* 11:195-212

Greco R, Sorriso-Valvo M, Catalano E (2007) Logistic regression analysis in the evaluation of mass-movements susceptibility-the Aspromonte case study, Calabria. *Eng Geol* 89:47-66

Gullà G (2014) Field monitoring in sample sites: hydrological response of slopes with reference to widespread landslide events. *Procedia Earth and Planetary Science* 9:44-53

Gullà G, Antronico L, Borrelli L, Cilento M, Aceto L, Scionti V (2006) Relazione Finale -Parti I-II-III e Cartografia. Convenzione di consulenza tecnico-scientifica Esecuzione di un programma di studi ed indagini finalizzati alla individuazione delle cause che hanno determinato la gravissima situazione di dissesto idrogeologico nel territorio del Comune di Lungro (CS). CNR-IRPI, OPCM n. 3460/2005. Unpublished report, (in Italian)

Gullà G, Niceforo D, Bonci L, Calcaterra S, Cesi C, Gambino P (2004) Surface movements of a landslide involving weathered and degraded rocks. *Proc. of the 15<sup>th</sup> Southeast Asian Geotechnical Conference, November 22-26, 2004 (15<sup>th</sup> SEAGC), Bangkok, Thailand, Volume 1, 375-378*

Guzzetti F, Mondini A C, Cardinali M, Fiorucci F, Santangelo M, Chang KT (2012) Landslide inventory maps: new tools for and old problem. *Earth-Sci Rev* 112:42-66

Herrera G, Gutierrez F, Garcia-Davalillo JC, Guerrero J, Notti D, Galve JP, Fernandez-Merodo JA, Cooksley G (2013) Multi-sensor advanced DInSAR monitoring of very slow landslides: The Tena Valley case study (Central Spanish Pyrenees). *Remote Sens Environ* 128:31-43

Iannace A, Bonari G, D'Errico M, Mazzoli S, Perrone V, Vitale S (2005) Structural setting and tectonic evolution of the Apennine Units of northern Calabria. *C.R. Geoscience* 337:1541-1550

Kim HW (2008) Development of wireless sensor node for landslide detection, in *Landslides and Engineered Slopes*, Chen et al. (eds), Taylor & Francis Group, London, ISBN 978-0-415-41196-7, 1183-1187

Komac M, Holley R, Mahapatra P, van der Marel H, Bavec M (2015) Coupling of GPS/GNSS and radar interferometric data for a 3D surface displacement monitoring of landslides. *Landslides* 12:241-257

Kumsar H, Aydan O, Tano H, Celik SB, Ulusay R (2015) An Integrated Geomechanical Investigation, Multi-Parameter Monitoring and Analyses of Babadag~ -Gu~ndog~du Creep-like Landslide. *Rock Mech Rock Eng.* doi:10.1007/s00603-015-0826-7

Laribi A, Walstra J, Ougrine M, Seridi A, Dechemi N (2015) Use of digital photogrammetry for the study of unstable slopes in urban areas: Case study of the El Biar landslide, Algiers. *Eng Geol* 187:73-83

Lu P, Catani F, Tofani V, Casagli N (2014) Quantitative hazard and risk assessment for slow-moving landslides from Persistent Scatterer Interferometry. *Landslides* 11:685-696

*Geometric and kinematic characterization of landslides affecting urban areas: the Lungro case study (Calabria, Southern Italy). Gullà G., Peduto D., Borrelli L., Antronico L., Fornaro G. (2017)*

Maiorano SC, Borrelli L, Moraci N, Gullà G, (2015) Numerical modelling to calibrate the geotechnical model of a deep-seated landslide in weathered crystalline rocks: Acri (Calabria, Italy). G. Lollino et al. (eds.), Engineering Geology for Society and Territory – Volume 2, pp 1271-1274

Massey CI, Petley DN, McSaveney MJ (2013) Patterns of movement in reactivated landslides. Eng Geol 159:1-19

MATTM (2010) Piano Straordinario di Telerilevamento Ambientale (PSTA). Linee guida per l'analisi dei dati interferometrici satellitari in aree soggette a dissesti idrogeologici, Italian Ministry of the Environment and Protection of Land and Sea (MATTM), pp 108

Meisina C, Zucca F, Notti D, Colombo A, Cucchi A, Savio G, Giannico C, Bianchi M (2008) Geological Interpretation of PSInSAR Data at Regional Scale. Sensors 8:7469-7492

Nico G, Borrelli L, Di Pasquale A, Antronico L, Gullà G (2015) Monitoring of an ancient landslide phenomenon by GBSAR technique in the Maierato town (Calabria, Italy). G. Lollino et al. (eds.), Engineering Geology for Society and Territory – Volume 2, pp 129-133

Notti D, Davalillo JC, Herrera G, Mora O (2010) Assessment of the performance of X-band satellite radar data for landslide mapping and monitoring: Upper Tena Valley case study. Nat Hazards Earth Syst Sci 10:1865-1875

Peduto D, Arena L, Calvello M, Anzalone R, Cascini L (2015). Evaluating the state of activity of slow-moving landslides by means of DInSAR data and statistical analyses. In Proc of the XVI ECSMGE Geotechnical Engineering for Infrastructure and Development, ISBN 978-0-7277-6067-8, ICE Publishing, doi:10.1680/ecsmge.60678, Vol.4, pp. 1843-1848

Petley DN, Mantovani F, Bulmer MH, Zannoni A (2005) The use of surface monitoring data for the interpretation of landslide movement patterns. Geomorphology 66:133-147

Pilot G (1984) Instrumentation and warning system for research and complex slope stability problems. Proc. 4<sup>th</sup> Int. Symp. on Landslides, Toronto, I, pp 275-306

Rib HT, Liang T (1978) Recognition and identification. In: Landslide Analysis and Control, edited by: Schuster, R. L. and Krizek, R. J., National Academy of Sciences, Transportation Research Board Special Report 176, Washington, pp 34–80

Risknat Project (2012) Le tecniche radar interferometriche nella pianificazione territoriale, KC Edizioni, Genova, Italy, pp 188, ISBN: 978-88-89007-37-2

Sassa K, Picarelli L, Yueping Y (2009) Monitoring, prediction and early warning, in Sassa K., Canuti P. (eds), Landslides – Disaster Risk Reduction, Springer-Verlag Berlin Heidelberg, pp 351-375

Shimizu N, Nakashima S, Masunari T (2014) ISRM Suggested Method for Monitoring Rock Displacements Using the Global Positioning System (GPS). Rock Mech Rock Eng 47:313-328

Simeoni L, Mongiovì L (2007) Incliner monitoring of the Castelrotto landslide in Italy. J. Geotech Geoenviron Eng 133:653-666

Stark TD, Choi H (2008) Slope inclinometers for landslides. Landslides 5:339-350

TERRAFIRMA: available at: <http://www.terrafirma.eu.com>, last access: 9 April 2015

- Geometric and kinematic characterization of landslides affecting urban areas: the Lungro case study (Calabria, Southern Italy). Gullà G., Peduto D., Borrelli L., Antronico L., Fornaro G. (2017)*
- Terranova C, Iuliano S, Matano F, Nardò S, Piscitelli E, Cascone E, D'Argenio F, Gelli L, Alfinito M, Luongo G (2009) The TELLUS Project: a satellite-based slow-moving landslides monitoring system in the urban areas of Campania Region, Proceedings of the Conference on Geology and Information Technology, 3–5 June 2008, Offida (AP). *Rend Online Soc Geol It* 8:148-151
- Tofani V, Raspini F, Catani F, Casagli N (2013a) Persistent Scatterer Interferometry (PSI) Technique for Landslide Characterization and Monitoring. *Remote Sensing* 5:1045-1065
- Tofani V, Segoni S, Agostini A, Catani F, Casagli N (2013b) Technical Note: Use of remote sensing for landslide studies in Europe. *Nat Hazards Earth Syst Sci* 13:299-309
- Tommasi P, Pellegrini P, Boldini D, Ribacchi R (2006) Influence of rainfall regime on hydraulic conditions and movement rates in the overconsolidated clayey slope of the Orvieto hill (central Italy). *Can Geotech J* 43:70-86
- Uzielli M, Catani F, Tofani V, Casagli N (2015) Risk analysis for the Ancona landslide—I: characterization of landslide kinematics. *Landslides* 12:69-82
- Varnes DJ (1978) Slope Movement Types and Processes, in: Special Report 176: Landslides: Analysis and Control, edited by: Schuster, R. L. and Krizek, R. J., TRB, National Research Council, Washington, DC, pp 11-33
- Vaunat J, Leroueil S (2002) Analysis of Post-Failure Slope Movements within the Framework of Hazard and Risk Analysis. *Nat Hazards* 26:83-109
- Walstra J, Dixon N, Chandler JH (2007) Historic aerial photographs for landslide assessment: two case histories. *Q J Eng Geol Hydrogeol* 40:315-332
- Wang G (2012) Kinematics of the Cerca del Cielo, Puerto Rico landslide derived from GPS observations. *Landslides* 9:117-130
- Wang G, Kearns TJ, Yu J, Saenz G (2014) A stable reference frame for landslide monitoring using GPS in the Puerto Rico and Virgin Island region. *Landslides* 11:119-129
- Wasowski J, Bovenga F (2014) Investigating landslides and unstable slopes with satellite Multi Temporal Interferometry: Current issues and future perspectives. *Eng Geol* 174:103-138
- Wei M, Sandwell DT (2010) Decorrelation of L-band and C-band interferometry over vegetated areas in California. *IEEE Trans Geosci Remote Sens* 48:2942-2952
- Willenberg H, Loew S, Eberhardt E, Evans KF, Spillmann T, Heincke B, Maurer H, Green AG (2008) Internal structure and deformation of an unstable crystalline rock mass above Randa (Switzerland): Part I — Internal structure from integrated geological and geophysical investigations. *Eng Geol* 101:1-14
- Xiao R, He X (2013) Real-time landslide monitoring of Pubugou hydropower resettlement zone using continuous GPS. *Nat Hazards* 69:1647-1660
- Yenes M, Monterrubio S, Nespereira J, Santos G (2009) Geometry and kinematics of a landslide surface in tertiary clays from the Duero Basin (Spain). *Eng Geol* 104:41-54
- Yin Y, Zheng W, Liu Y, Zhang J, Li X (2010) Integration of GPS with InSAR to monitoring of the Jiaju landslide in Sichuan, China. *Landslides* 7:359-365

*Geometric and kinematic characterization of landslides affecting urban areas: the Lungro case study (Calabria, Southern Italy). Gullà G., Peduto D., Borrelli L., Antronico L., Fornaro G. (2017)*

Zanutta A, Baldi P, Bitelli G, Cardinali M, Carrara A (2006) Qualitative and quantitative photogrammetric techniques for multi-temporal landslide analysis. *Ann Geophys* 49:1067-1080

## **List of Figure and Table captions**

Fig. 1 Geological sketch of northern Calabria (from Iannace et al., 2005 modified) and geological map of the study area. Legend: (1) alluvial deposits (Holocene); (2) detritical carbonate deposits (Holocene); (3) detritical-colluvial cover (Holocene); (4) Middle Pliocene-Pleistocene succession; (5) Middle Tortonian-Messinian succession; (6) Diamante-Terranova Unit (Lower Jurassic-Cretaceous); (7) Lungro-Verbicaro Unit (Anisian-Lower Burdigalian); (8) tectonic contact; (9) analysed portions of the urban area (HC = Historical centre; CA = Carmine; LA = Lafcantino; SL = San Leonardo)

Fig. 2 Framework of the *a posteriori* (*aPosIn*) procedure

Fig. 3 Landslide inventory map of Lungro (a), categories of landslides (b), and analysed portions of the urban area (HC = Historic centre, LA = Lafcantino; CA = Carmine, SL = San Leonardo). Legend: (1) main scarp of ancient rock slide; (2) uncertain boundary of ancient rock slide; (3) boundary of active slide; (4) boundary of dormant slide; (5) boundary of active slide-flow; (6) boundary of dormant slide-flow; (7) boundary of active landslide zone; (8) category A; (9) category B; (10) category C; (11) category D

Fig. 4 A-DInSAR data distribution over the analysed portions of the urban area (HC = Historic centre, LA = Lafcantino; CA = Carmine, SL = San Leonardo). (a) Low-resolution A-DInSAR data distribution (descending-orbit data are distinguished from ascending-orbit data using black contoured circles). (b) Full-resolution A-DInSAR data distribution

Table 1 Representative A-DInSAR-based velocities in the Lungro urban area (HC = Historic centre, LA = Lafcantino; CA = Carmine, SL = San Leonardo)

Fig. 5 Average and maximum velocities based on GPS benchmark data and inclinometer data during the monitoring periods in the analysed portions of the urban area (HC = Historic centre, LA = Lafcantino; CA = Carmine, SL = San Leonardo). (a) GPS benchmark data, yearly average velocity class; (b) GPS benchmark data, maximum velocity class; (c) inclinometer data, yearly average velocity class; (d) inclinometer data, maximum velocity class

Fig. 6 Inclinometer measurements acquired from the deep displacement network from 2006 to 2011, in the analysed portions of the urban area (HC = Historic centre, LA = Lafcantino; CA = Carmine, SL = San Leonardo)

Table 2 Summary of minimum, average and maximum velocities at depths of 1 m based on inclinometer data

Table 3 Velocity classes based on previous studies in the Lungro urban area

Fig. 7 Integration of results from the *GeoG* and *Sat* methods in the analysed portions of the urban area (HC = Historic centre, LA = Lafcantino; CA = Carmine, SL = San Leonardo): (a) low-resolution A-DInSAR data; (b) full-resolution A-DInSAR data. Numbers in parentheses correspond to the landslide identification number

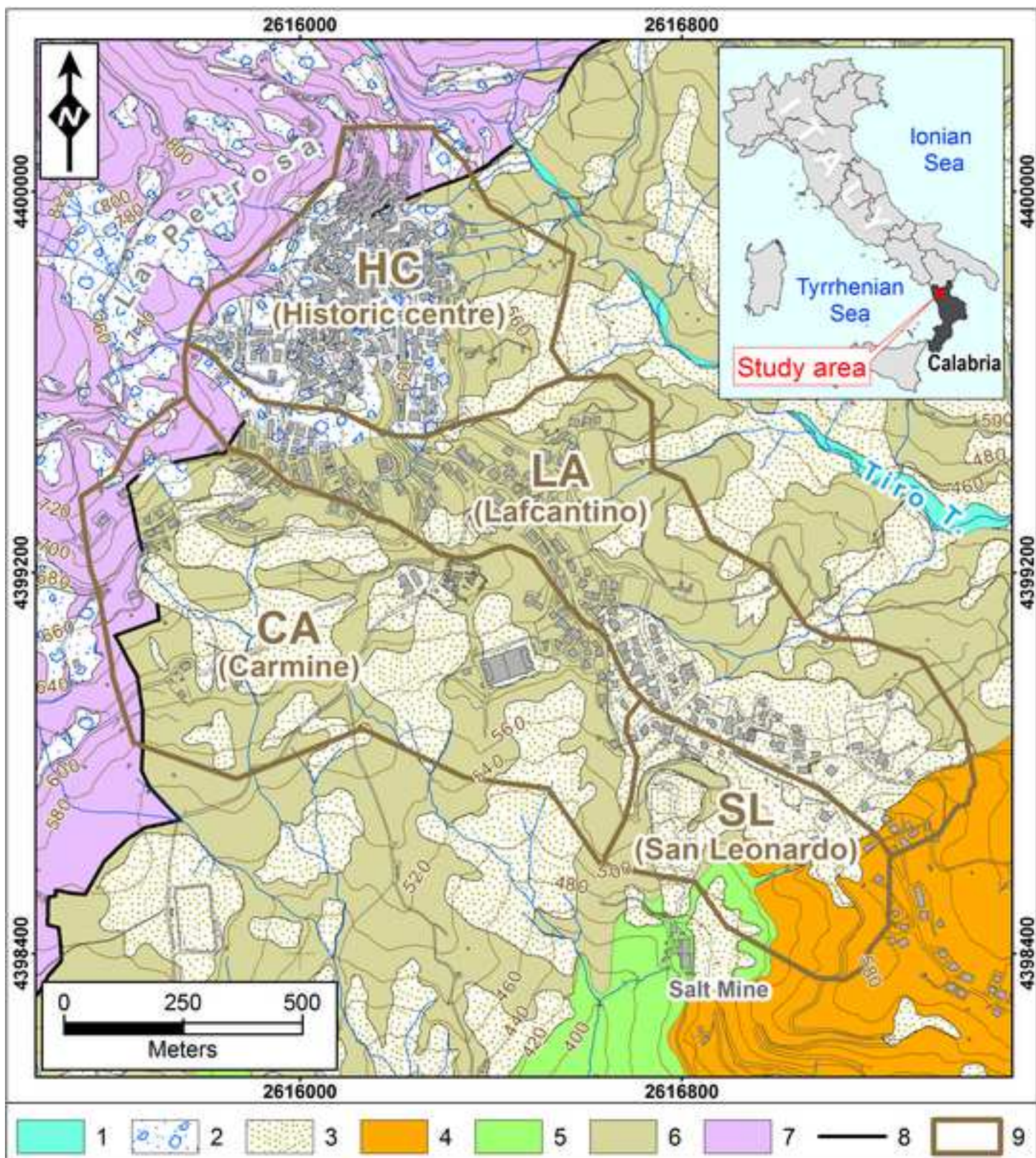
Fig. 8 Integration of the results from the *GeoG* and *Geot* methods in the analysed portions of the urban area (HC = Historic centre, LA = Lafcantino; CA = Carmine, SL = San Leonardo): (a) velocity classes; (b) thicknesses of the landslides. Numbers in parentheses correspond to the landslide identification number

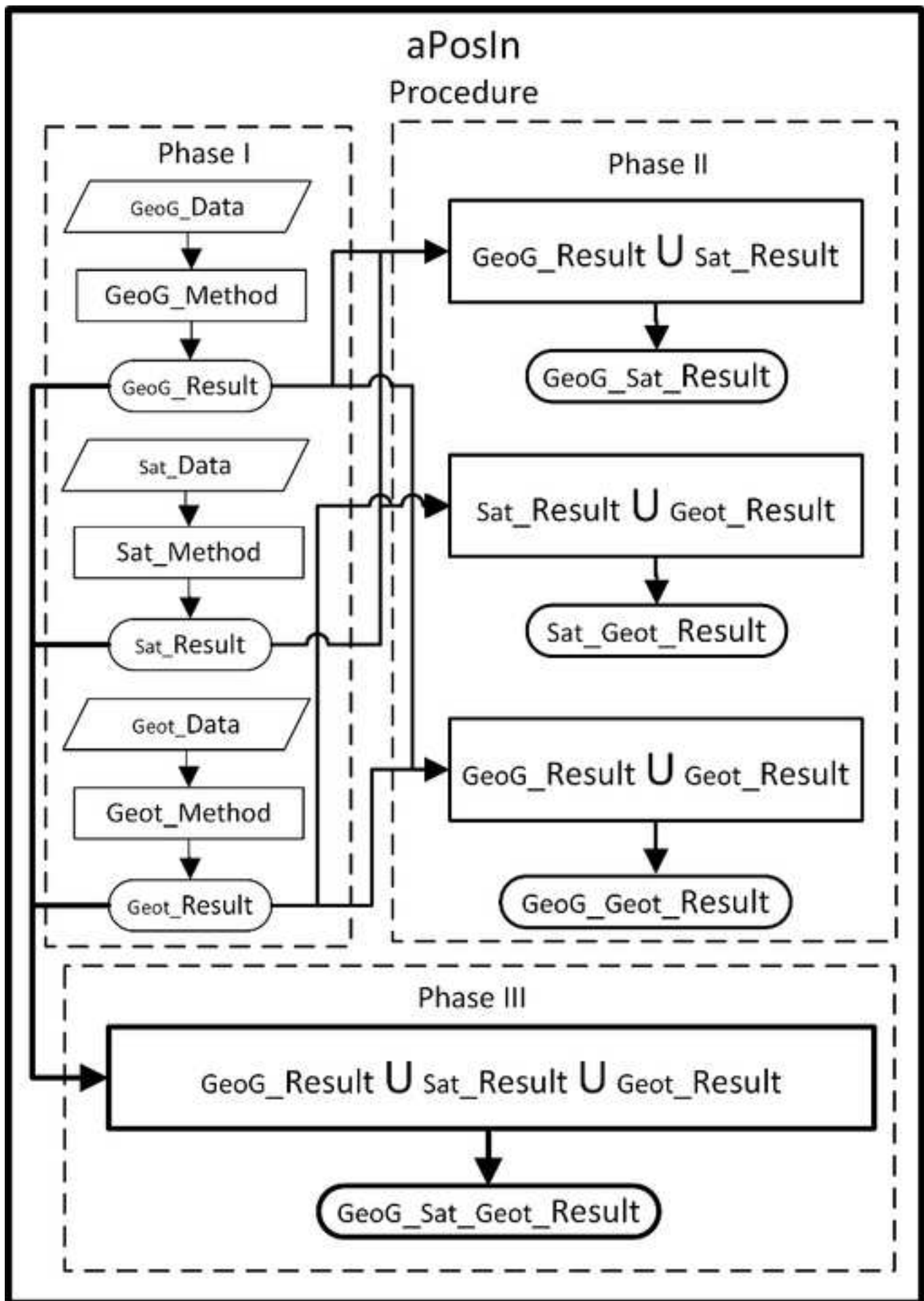
Fig. 9 Integration of results from the *Sat* and *Geot* methods in the analysed portions of the urban area (HC = Historic centre, LA = Lafcantino; CA = Carmine, SL = San Leonardo)

Fig. 10 Integration of results from the *GeoG*, *Sat* and *Geot* methods in the analysed portions of the urban area (HC = Historic centre, LA = Lafcantino; CA = Carmine, SL = San Leonardo), with landslide categories based on *GeoG* result and velocity classes based on A-DInSAR, GPS and inclinometer data. Numbers in parentheses correspond to the landslide identification number

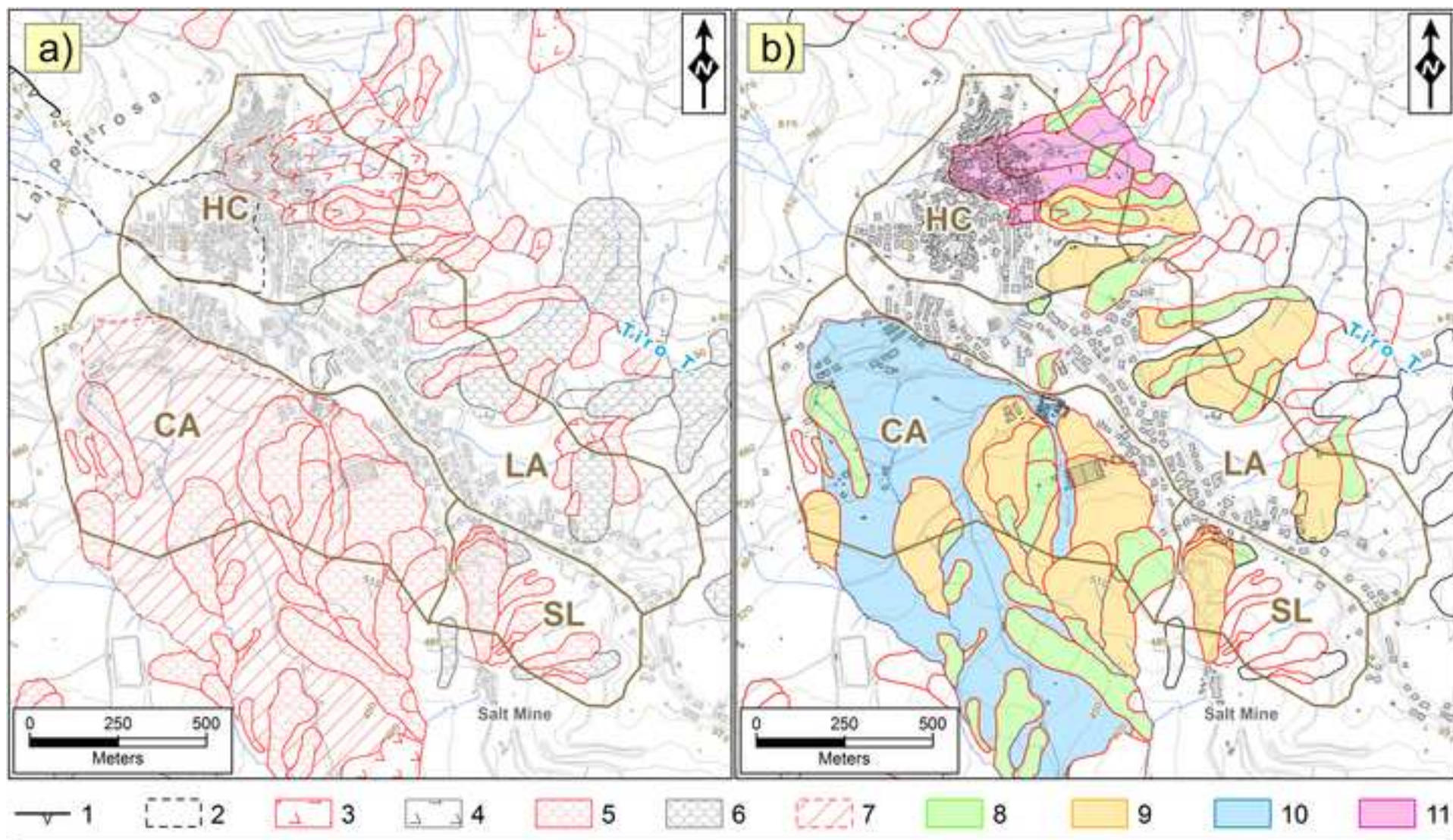
Fig. 11 Typified landslides defined based on the result of the *aPosIn* procedure. Numbers in parentheses correspond to the landslide identification number. Landslides directly typified are labelled in red; all the other landslides are labelled in black



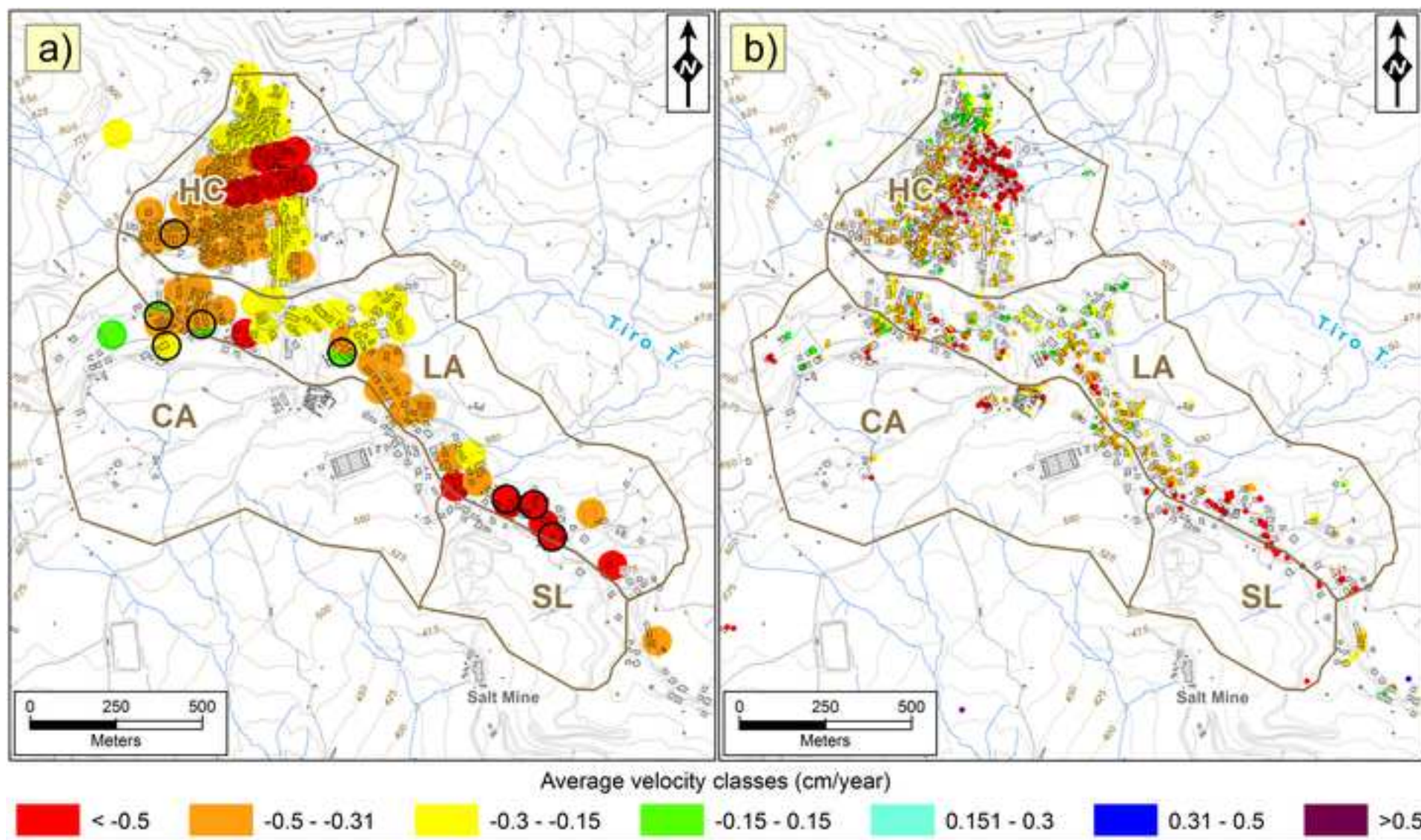




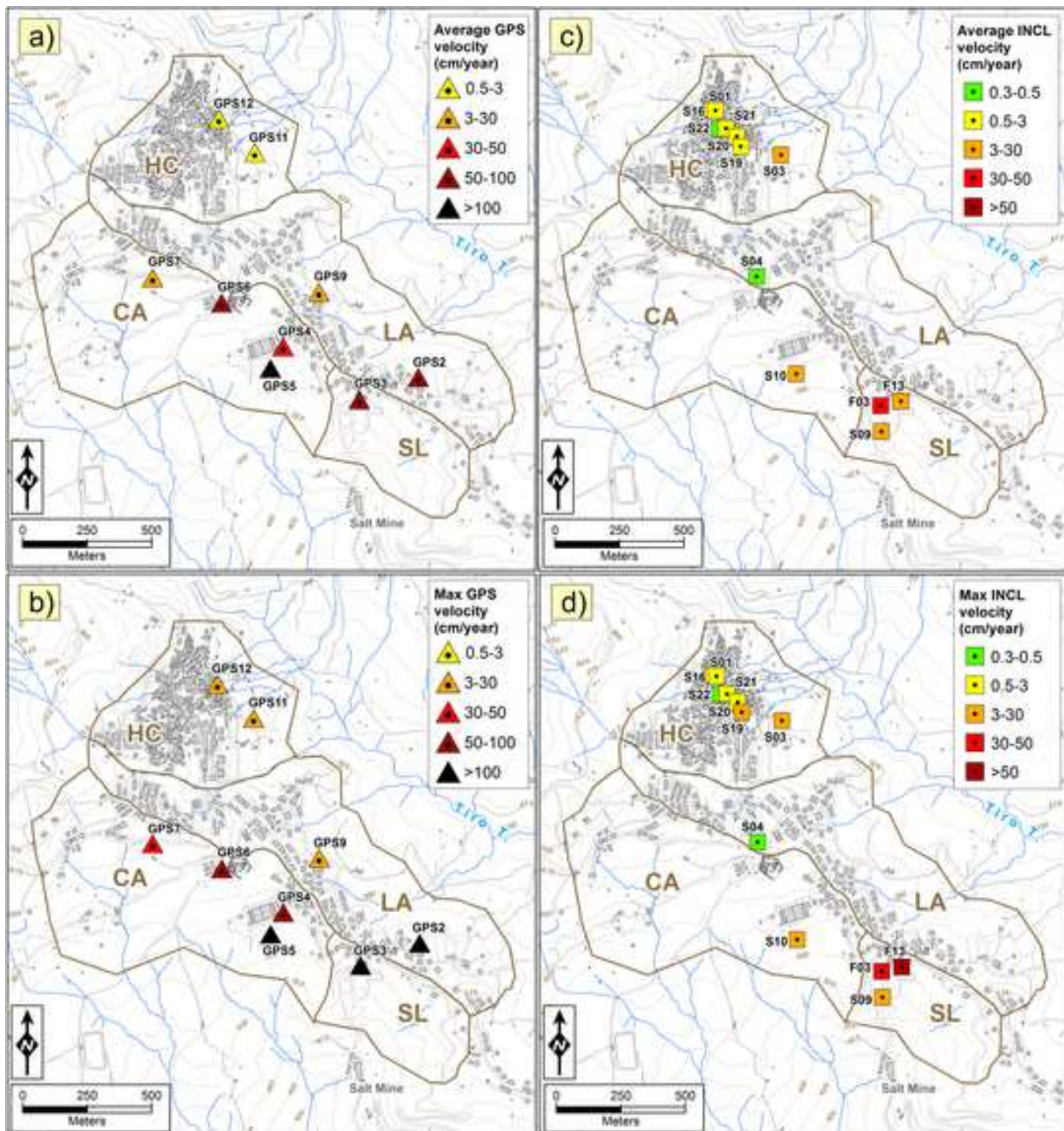


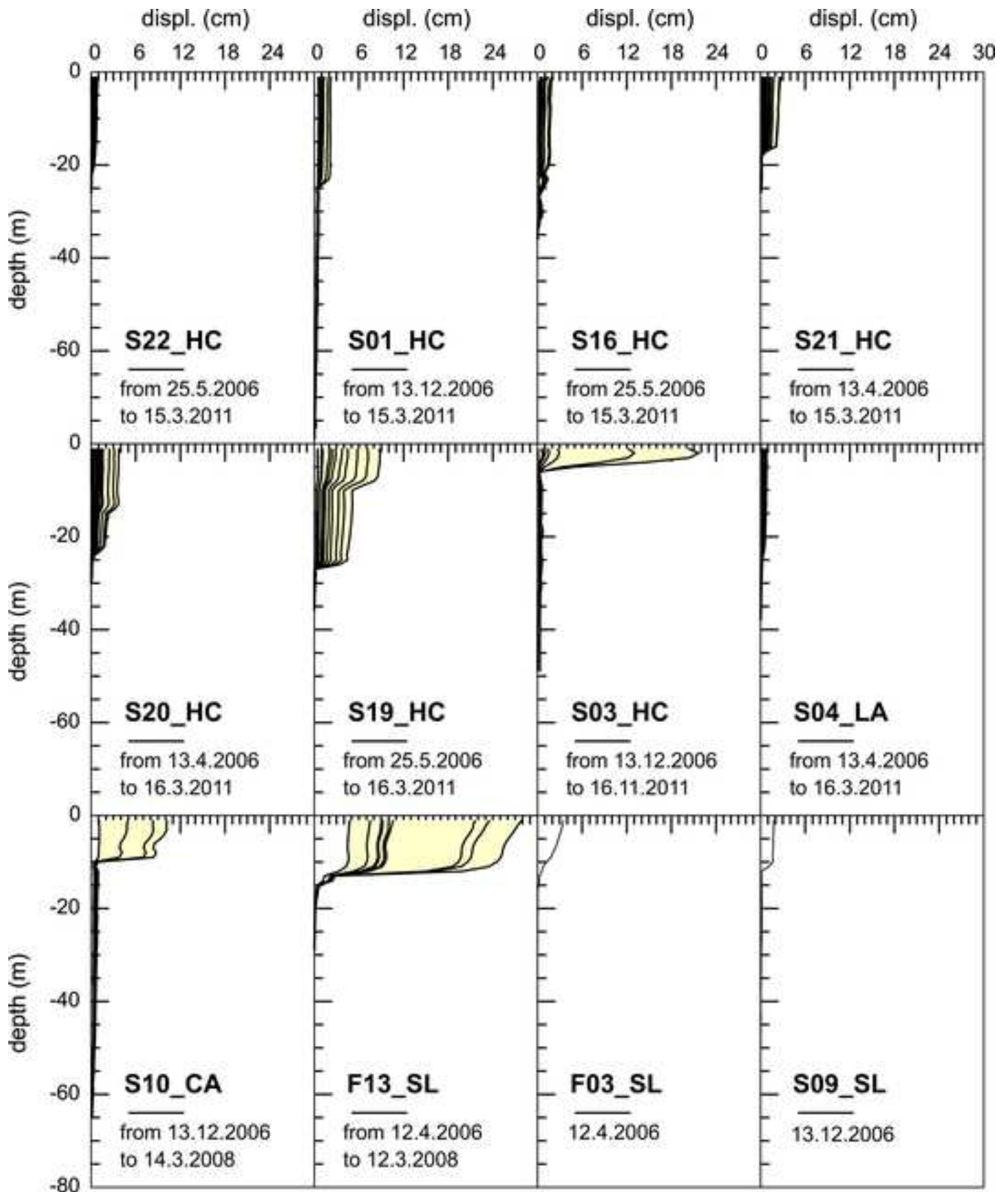




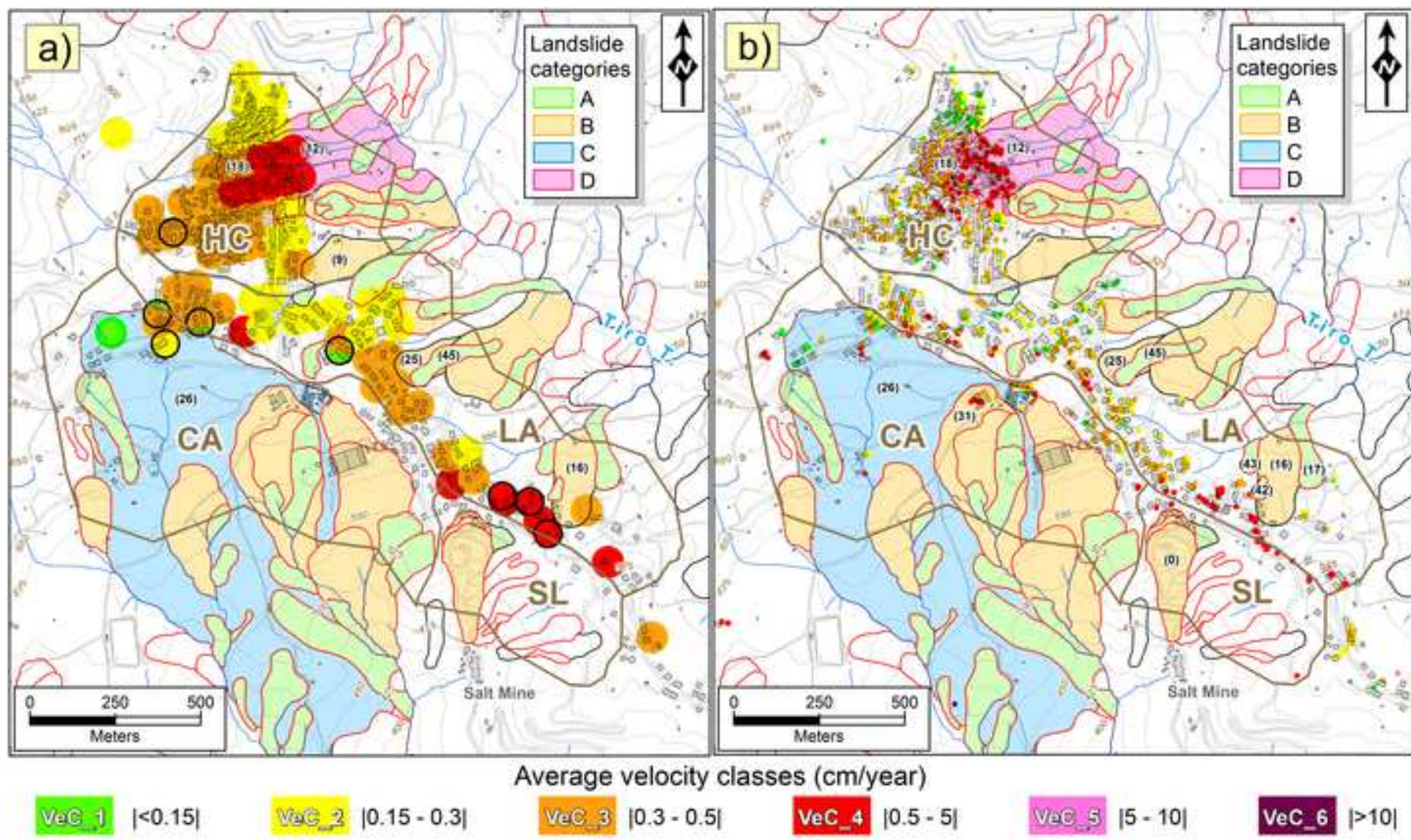




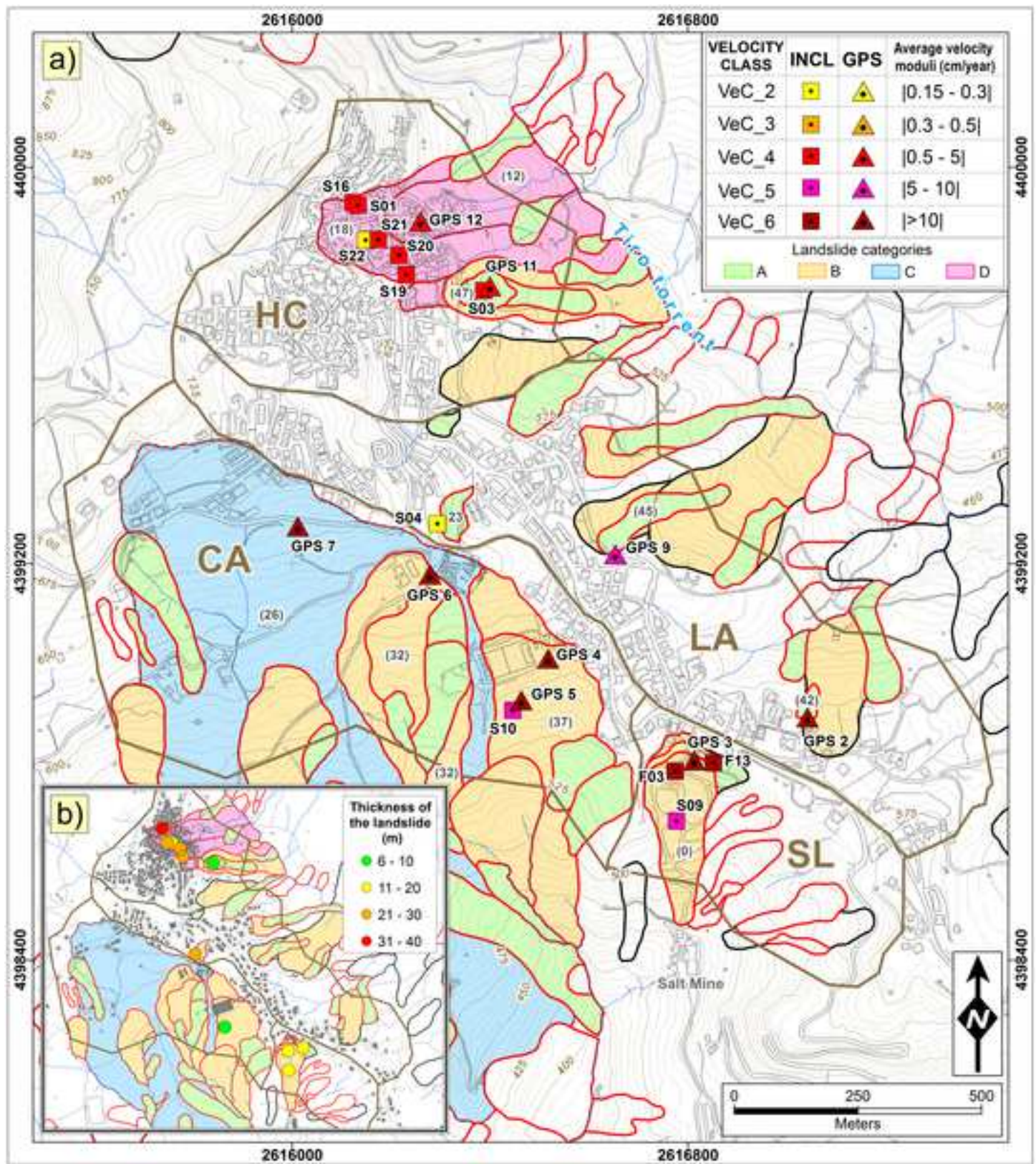




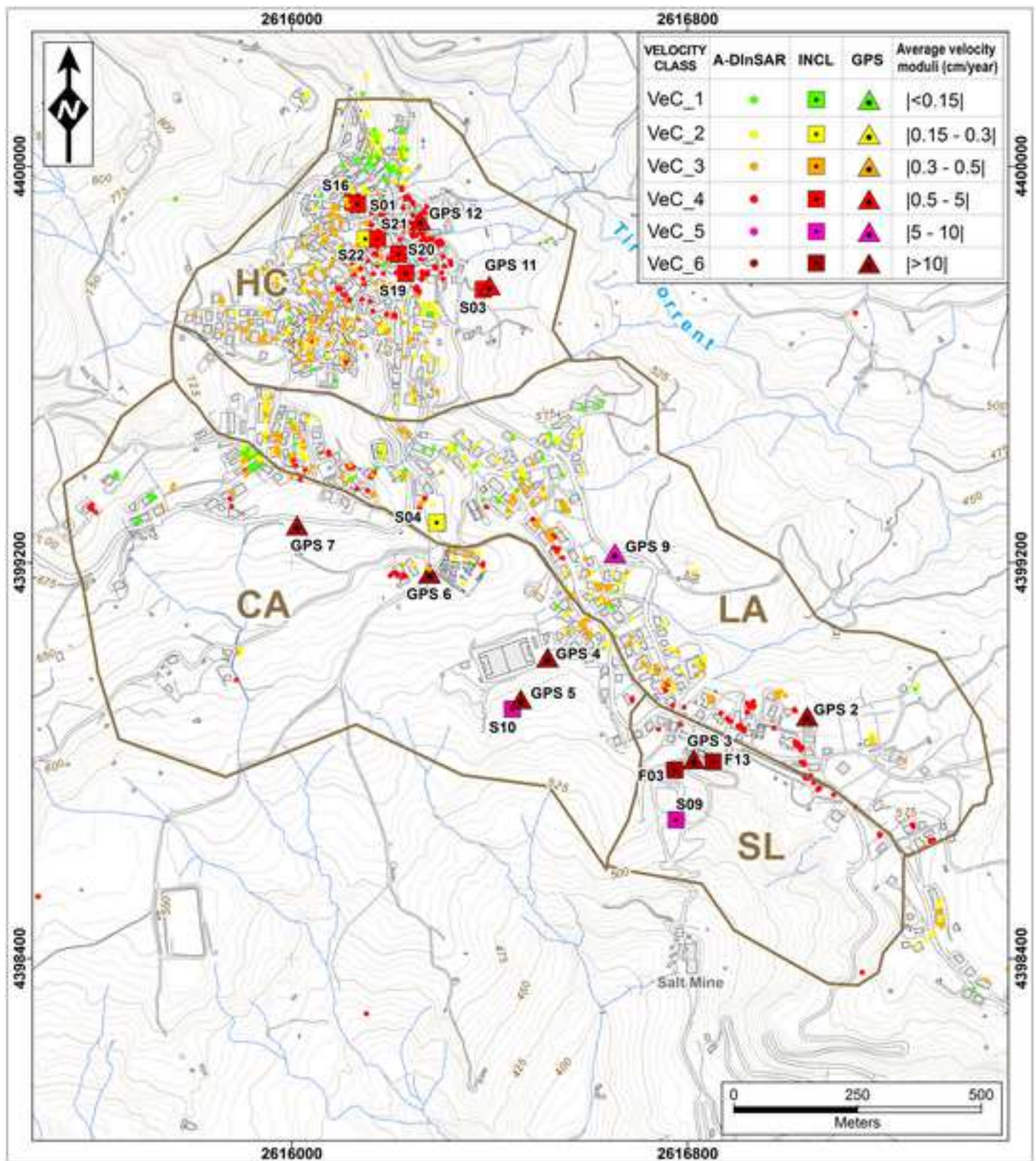




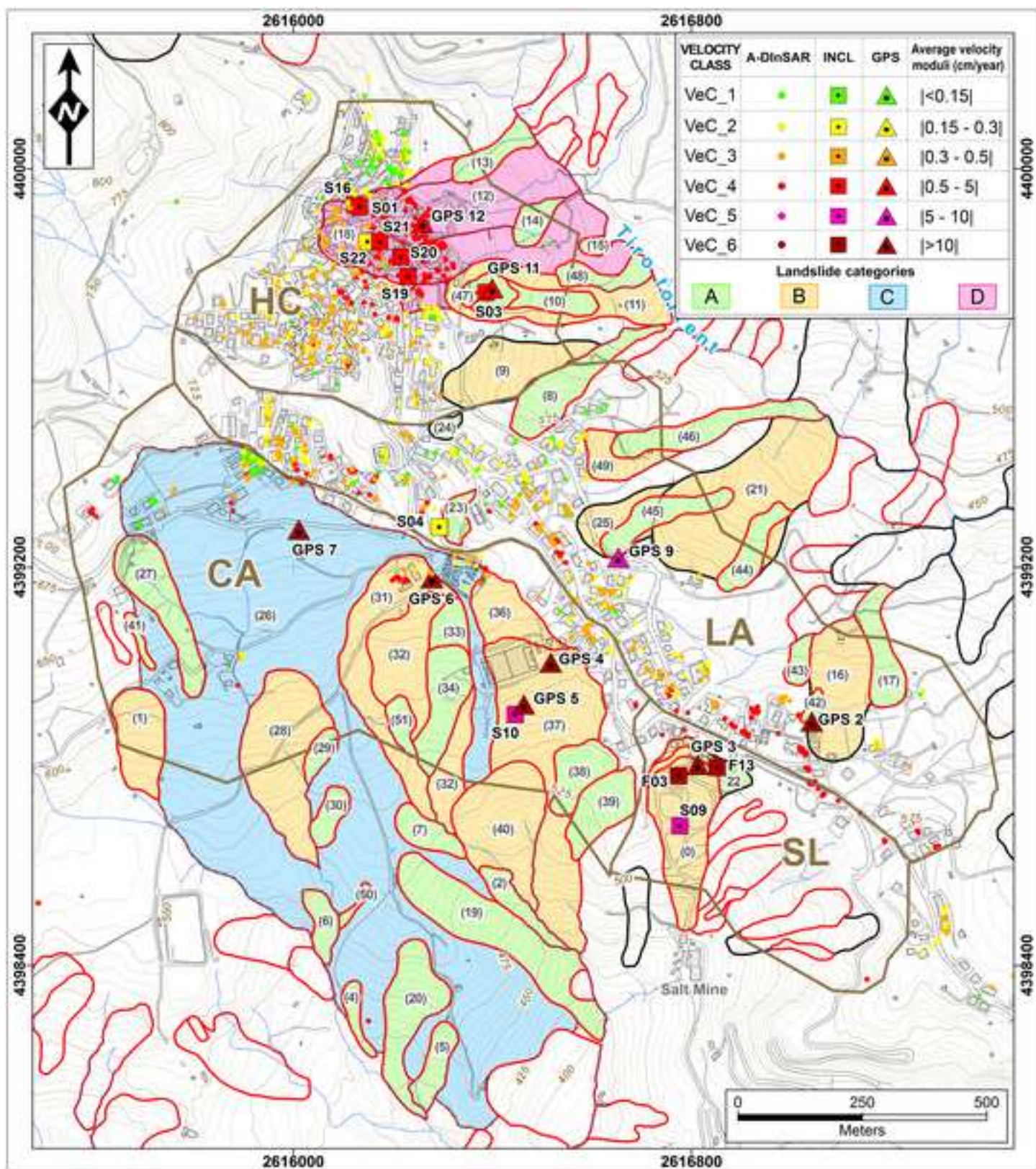




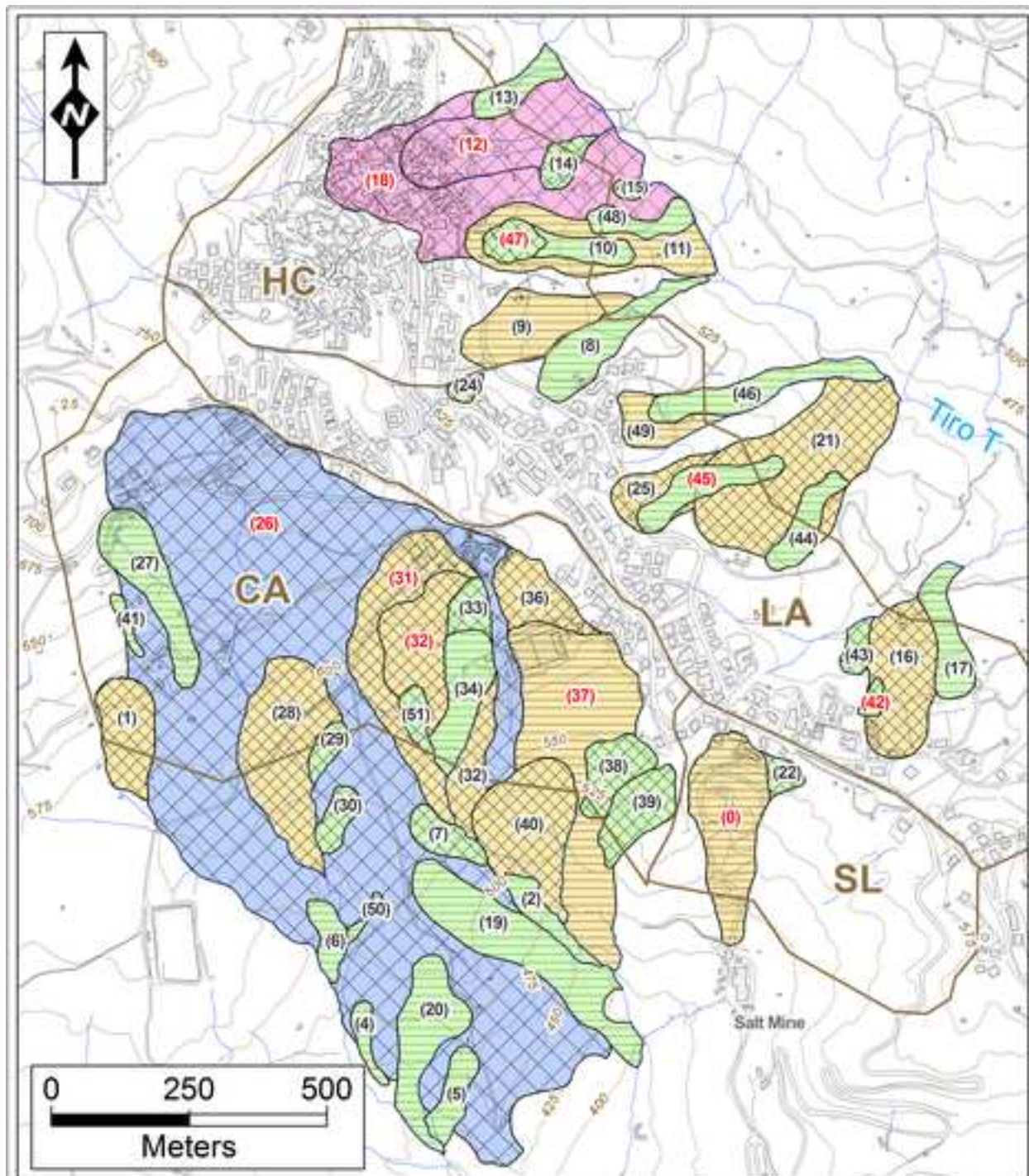



























LT	Width (W) [m]	Length (L) [m]	L/W	Depth [m]	Velocity [cm/year]		Geomaterial	kinematic_TYPE
					ordinary	critical		
T_A1	25-100	≤ 180	≤ 2.5	about 6	2-4	> 200	detritic-colluvial covers	complex landslide
T_A2	15-100	≥ 80	> 2.5	about 10	5-7	> 20		
T_B1	90-260	130-550	< 2.5	10-20	0.5-5	> 80	deeply weathered and chaotic phyllites	complex landslide
T_B2	80-220	> 300	≥ 2.5	10-16	4-20	> 100		
T_C	830	1500	1.8	20-30	0.5-5	> 40	deeply weathered and chaotic phyllites	landslide zone
T_D	100-250	350-550	2.2-3.2	20-30 / 10-15	0.2-0.5	2-5	weathered and chaotic phyllites	slide

<b>Ascending orbit</b>		<b>Descending orbit</b>	
<b>HC (Historic centre)</b>			
Number of Pixels	492	Number of Pixels	5
Minimum velocity [cm/year]	-1,34	Minimum velocity [cm/year]	-0,24
Maximum velocity [cm/year]	-0,05	Maximum velocity [cm/year]	0,05
Average velocity [cm/year]	-0,45	Average velocity [cm/year]	-0,07
Standard Deviation	0,28	Standard Deviation:	0,11
<b>LA (Lafcantino)</b>			
Number of Pixels	341	Number of Pixels	63
Minimum velocity [cm/year]	-1,51	Minimum velocity [cm/year]	-1,74
Maximum velocity [cm/year]	-0,03	Maximum velocity [cm/year]	0,11
Average velocity [cm/year]	-0,41	Average velocity [cm/year]	-0,42
Standard Deviation:	0,23	Standard Deviation:	0,47
<b>CA (Carmine)</b>			
Number of Pixels	79	Number of Pixels	57
Minimum velocity [cm/year]	-0,98	Minimum velocity [cm/year]	-0,73
Maximum velocity [cm/year]	-0,03	Maximum velocity [cm/year]	0,02
Average velocity [cm/year]	-0,39	Average velocity [cm/year]	-0,19
Standard Deviation:	0,22	Standard Deviation:	0,14
<b>SL (San Leonardo)</b>			
Number of Pixels	10	Number of Pixels	7
Minimum velocity [cm/year]	-1,56	Minimum velocity [cm/year]	-2,29
Maximum velocity [cm/year]	-0,68	Maximum velocity [cm/year]	-0,58
Average velocity [cm/year]	-1,21	Average velocity [cm/year]	-1,62
Standard Deviation:	0,33	Standard Deviation:	0,65

Portions of the urban area	Inclinometer	v [cm/year]		
		min	average	max
HC (Historic centre)	S01	0.13	0.68	2.50
	S03	0.06	3.89	13.07
	S16	0.10	0.54	1.55
	S19	0.48	1.99	4.97
	S20	0.03	0.72	1.88
	S21	0.17	0.64	1.62
	S22	0.05	0.18	0.35
LA (Lafcantino)	S04	0.06	0.24	0.39
CA (Carmine)	S10	4.65	6.66	9.17
SL (San Leonardo)	F03	—	36.60	—
	S09	5.85	9.95	16.21
	F13	3.60	18.45	51.10

Velocity Classes	Ranges of the average yearly velocity moduli (cm/year)	<i>Sat</i>	<i>Geot (INCL)</i>	<i>Geot (GPS)</i>
VeC_01	<0.15			
VeC_02	0.15-0.3			
VeC_03	0.3-0.5			
VeC_04	0.5-5			
VeC_05	5-10			
VeC_06	>10	